

THE STATE OF THE ART ON NUMERICAL WAVE TANK

Katsuji TANIZAWA

Ship Research Institute

Tokyo, JAPAN

ABSTRACT

The present theoretical and technological state of numerical wave tank (NWT) is explained. In the past two decades, many researchers have studied time domain simulation methods of nonlinear free surface and floating body motions. Through these studies, theories and numerical techniques were developed. The accumulation of these knowledge lies at the base of present NWTs. In this article, these theories, numerical techniques and useful ideas for NWT are categorized and instructed with mathematical formulations.

KEY WORDS: Numerical wave tank, mixed Eulerian and Lagrangian method, boundary element method, boundary integral equation, time domain simulation, nonlinear wave, nonlinear floating body dynamics, acceleration potential

1 INTRODUCTION

Numerical Wave Tank (NWT) is a generic name of numerical simulators for nonlinear free surface waves, hydrodynamic forces and floating body motions. In the past two decades, a lot of efforts have been made to develop theories and numerical techniques for NWT.

The first pioneer work was the development of well known mixed Eulerian and Lagrangian method (MEL) by Longuet-Higgins and Cokelet (1976). In MEL method, as its name shows, Eulerian field equations are solved to obtain fluid velocity, and obtained velocity is used to track fluid particles on the free surface in Lagrangian way. The development of MEL enabled us to compute fully nonlinear free surface motions in time domain. Initiated by this work, many MWTs were developed to simulate nonlinear free surface motions and hydrodynamic forces acts on fixed bodies. Dommermuth et al. (1988) developed 2D NWT based on complex potential and simulated deep water plunging waves, Xu and Yue (1992) developed 3D NWT and simulated 3D

overturning waves, Grilli et al. (2000) also simulated 3D overturning waves over arbitrary bottom in 3D NWT. Zhang et al. (1996) simulated plunging wave impact force on a vertical wall. Boo and Kim (1996,1997) simulated nonlinear wave diffraction force on vertical circular cylinder. Ferrant (1998) simulated fully nonlinear run up of water on a cylinder due to wave and current.

The second pioneer work was the development of modal decomposition method by Vinje and Brevig (1981a, 1981b). They introduced acceleration field and showed how to determine pressure distribution and resulting floating body acceleration simultaneously. This was the first consistent method to simulate nonlinear floating body motions in time domain. Cointe et al.(1990) used this method in their NWT. Following these works, other three consistent methods were developed in rapid succession. Tanizawa (1990,1995a) developed implicit boundary condition method. Berkvens (1998) developed 3D NWT based on this method. Recently, Ikeno (2000) and Shirakura (2000) also developed 3D NWT based on implicit boundary condition method. Cao (1994) developed iterative method. Wu and Eatock-Taylor (1996) extended the modal decomposition method and proposed a new indirect method. Kashiwagi (1998) used this method as the fastest solver of floating body motions.

By these research efforts, theories and numerical techniques were developed and prepared as necessary parts of NWT. Nowadays, using these parts, we can develop practical 2D NWT as we wish. On the other hand, development of practical 3D NWT is still tough work. We have to develop additional theories and various numerical techniques for 3D NWT. Desktop computers are still not powerful enough to run 3D simulations. However, development of 3D NWT is present hot topic. Many challenging works are on going and overcoming the difficulties.

The aim of this article is presenting theories and numerical techniques for NWT. Although the viscous fluid NWT is equally as important as ideal fluid NWT, the author limited the contents to ideal fluid NWT only

and tried to give instructions as briefly as possible so that readers can imagine some plans to develop their own NWT. However, the target readers are not limited to young researchers or new NWT developer. The author expects that this article is also useful for mature researchers to find a new meaning of nonlinear floating body dynamics in the acceleration field. Designers of ships and ocean structures are also the target. They will understand the present state of NWTs and find good applications.

On the other hand, this article is not a wide sequential review of published papers on NWT. Accordingly, the author picked up limited papers considered to be essentially important for the development of NWT. The presented new theories, new ideas and new numerical techniques were categorized and explained in appropriate sections with mathematical formulas. However, many interesting papers concerning on the application of NWT were omitted. Readers might feel that something is missing. Wide review of published papers on NWT was presented by Kim et al. (1999). The author recommends to read this paper for wider understanding of NWT.

At the end of introduction, definition of NWT is clarified. **NWT is a computer code which final goal is to reproduce physical wave tanks as closely as possible.** The minimum requirements of NWT adopted by NWT group of International Society of Offshore and Polar Engineers are support of following items.

- Simulation of free surface waves dominated by gravity,
- Fully nonlinear boundary conditions applied on both free surface and body surface,
- Simulation in a bounded domain,
- Simulation in time domain,
- Physical wave generation (moving wall or varying pressure).

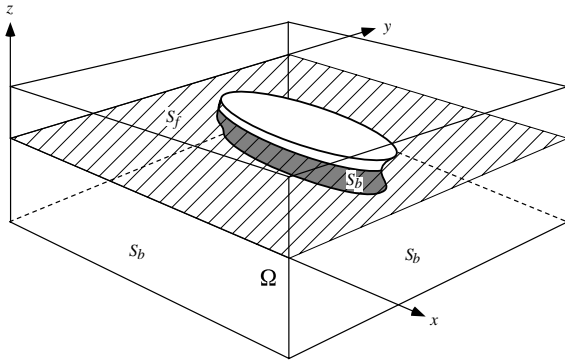


Fig.1 Fluid domain bounded by free surface and body surface

2 THEORETICAL BACKGROUND OF NWT

2.1 BOUNDARY INTEGRAL EQUATIONS

In this article, the fluid is assumed to be homogeneous, incompressible, inviscid and its motion irrotational. All variables are nondimensionalized using fluid density ρ , gravitational acceleration g and characteristic length on NWT L . To describe the ideal fluid

motion, the velocity potential is popularly used. For two dimensional problem, the complex potential is also a good choice. Using velocity potential or complex potential, boundary integral equations (BIE) are formulated as follows.

Fig.1 shows a 3D fluid domain bounded by free surface S_f and body surface S_b . The space fixed coordinate $x - y - z$ is used to figure out 3D domain. For 2D domain, $x - z$ is used. In both system, z is positive upward and $z = 0$ coincides with calm water surface. In the fluid domain, the velocity potential satisfies Laplace's equation.

$$\nabla^2 \phi = 0 \quad (1)$$

Applying Green's theorem, we have

$$c(Q)\phi(Q) = \int_S \phi(P)u_n(P, Q) - u(P, Q)\phi_n(P)ds, \quad (2)$$

where P and Q are points on the boundary $S = S_f \cup S_b$, $c(Q)$ is solid angle of the boundary at point Q , $u(P, Q)$ is kernel function and subscript n denotes the operation $\mathbf{n} \cdot \nabla$ in which \mathbf{n} is the unit surface normal vector. In this article, subscript x, y, z, s , etc. also denotes the same kind of operation in each direction. Kernel function $u(P, Q)$ is written as

$$u(P, Q) = \begin{cases} -\ln \|P - Q\| & \text{for 2D problem} \\ 1/\|P - Q\| & \text{for 3D problem} \end{cases} \quad (3)$$

where $\|P - Q\|$ is the distance between P and Q.

The complex potential is defined as $\beta(Z, t) = \phi(Z, t) + i\psi(Z, t)$, where $Z = x + iz$ and ψ is the stream function. ψ also satisfies Laplace's equation.

$$\nabla^2 \psi = 0 \quad (4)$$

Since β is analytic inside the fluid domain, Cauchy's integral theorem can be applied.

$$2\pi i \beta(Z_o) = \int_S \frac{\beta(Z)}{Z - Z_o} dZ, \quad (5)$$

Now, let Z_o approach S , Fredholm integral equations of the second kind for ϕ on S_b and ψ on S_f are obtained.

$$\left. \begin{aligned} c(Z_o)\psi(Z_o) + \Re \left\{ \int_S \frac{\beta(Z)}{Z - Z_o} dZ \right\} &= 0 \quad \text{on } S_f \\ c(Z_o)\phi(Z_o) + \Re \left\{ \int_S \frac{\beta(Z)}{Z - Z_o} dZ \right\} &= 0 \quad \text{on } S_b \end{aligned} \right\} \quad (6)$$

Notice that these BIEs (2),(6) are valid when ϕ and ψ are replaced by $\partial\phi/\partial t \equiv \phi_t$ and $\partial\psi/\partial t \equiv \psi_t$ respectively.

2.2 BOUNDARY CONDITIONS OF VELOCITY AND ACCELERATION FIELDS

2.2.1 Free surface boundary condition

On S_f , dynamic free surface boundary condition is given as

$$\phi_t + \frac{1}{2} \nabla \phi \cdot \nabla \phi + z = 0. \quad (7)$$

Integrating this condition by so called MEL method, value of ϕ is given on S_f . MEL method is explained later in §2.4. The value of ϕ_t on S_f is simply calculated from this dynamic condition.

2.2.2 Body surface boundary condition

On body surface S_b , ϕ_n is given for BIE (2) and ψ is given for BIE (6). Let us denote translating velocity and angular velocity of the body as \mathbf{V} and $\boldsymbol{\omega}$ respectively. Then, ϕ_n on the body surface is given as

$$\phi_n = \mathbf{n} \cdot (\mathbf{V} + \boldsymbol{\omega} \times \mathbf{r}), \quad (8)$$

where \mathbf{r} is position vector of body surface with respect to the center of rotation. In 2D case, value of ψ is obtained by integrating ϕ_n along body surface. The integral constant can be determined as a part of the solution of BIE (6).

Next, let us focus on fluid acceleration and derive the body surface boundary condition of ϕ_t . Fluid acceleration \mathbf{a} is material derivative of fluid velocity \mathbf{v} .

$$\mathbf{a} = \frac{D\mathbf{v}}{Dt} = \frac{\partial \mathbf{v}}{\partial t} + (\mathbf{v} \cdot \nabla) \mathbf{v}, \quad (9)$$

where D/Dt means material derivative. Taking the relation $\mathbf{v} = \nabla\phi$ into account, eq.(9) is transformed to

$$\mathbf{a} = \nabla \left(\phi_t + \frac{1}{2} \nabla\phi \cdot \nabla\phi \right). \quad (10)$$

Thus, fluid acceleration is given as gradient of scalar function in the parenthesis. Tanizawa (1995) define this scalar function as nonlinear acceleration potential

$$\Phi = \phi_t + \frac{1}{2} \nabla\phi \cdot \nabla\phi, \quad (11)$$

and systematically derived following body surface boundary condition for Φ .

$$\begin{aligned} \Phi_n &= \mathbf{n} \cdot (\dot{\mathbf{V}} + \dot{\boldsymbol{\omega}} \times \mathbf{r}) \\ &\quad - k_n (\nabla\phi - \mathbf{V} - \boldsymbol{\omega} \times \mathbf{r})^2 \\ &\quad + \mathbf{n} \cdot \boldsymbol{\omega} \times (\boldsymbol{\omega} \times \mathbf{r}) \\ &\quad + \mathbf{n} \cdot 2\boldsymbol{\omega} \times (\nabla\phi - \mathbf{V} - \boldsymbol{\omega} \times \mathbf{r}), \end{aligned} \quad (12)$$

where $\dot{\mathbf{V}}$ and $\dot{\boldsymbol{\omega}}$ are translating and angular acceleration of the body respectively and k_n is normal curvature of the body surface. The four right side terms respectively arise from floating body acceleration, centripetal acceleration of flow along the curved body surface, centripetal acceleration due to angular velocity of the body and Coriolis acceleration. From eq.(11) and (12), body surface boundary condition for ϕ_t is obtained as follows.

$$\phi_{tn} = \mathbf{n} \cdot (\dot{\mathbf{V}} + \dot{\boldsymbol{\omega}} \times \mathbf{r}) + q \quad (13)$$

$$\begin{aligned} q &= -k_n (\nabla\phi - \mathbf{V} - \boldsymbol{\omega} \times \mathbf{r})^2 \\ &\quad + \mathbf{n} \cdot \boldsymbol{\omega} \times (\boldsymbol{\omega} \times \mathbf{r}) \\ &\quad + \mathbf{n} \cdot 2\boldsymbol{\omega} \times (\nabla\phi - \mathbf{V} - \boldsymbol{\omega} \times \mathbf{r}) \\ &\quad - \frac{\partial}{\partial n} \left(\frac{1}{2} \nabla\phi \cdot \nabla\phi \right) \end{aligned} \quad (14)$$

Here, q represent the contribution of velocity field to the acceleration field and its all terms are explicitly calculated from ϕ .

Denoting the generalized acceleration of the body as $\boldsymbol{\alpha} = (\dot{\mathbf{V}}, \dot{\boldsymbol{\omega}})$ and the generalized normal vector of body surface as $\mathbf{N} = (\mathbf{n}, \mathbf{r} \times \mathbf{n})$, eq.(13) can be written as

$$\phi_{tn} = \mathbf{N} \cdot \boldsymbol{\alpha} + q = \sum_{j=1}^6 \alpha_j N_j + q. \quad (15)$$

To evaluate the normal derivative of the velocity-squared term in q , Tanizawa (1995) gave following relation for 2D computation,

$$\begin{aligned} \frac{\partial}{\partial n} \left(\frac{1}{2} \nabla\phi \cdot \nabla\phi \right) &= -k_1 (\phi_n^2 + \phi_{s_1}^2) \\ &\quad - \phi_n \phi_{s_1 s_1} + \phi_{s_1} \phi_{s_1 n}, \end{aligned} \quad (16)$$

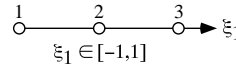
and Berkvens (1998) extended it for 3D computation,

$$\begin{aligned} \frac{\partial}{\partial n} \left(\frac{1}{2} \nabla\phi \cdot \nabla\phi \right) &= -(k_1 + k_2) \phi_n^2 - k_1 \phi_{s_1}^2 - k_2 \phi_{s_2}^2 \\ &\quad - (\phi_{s_1 s_1} + \phi_{s_2 s_2}) \phi_n \\ &\quad + \phi_{s_1} \phi_{s_1 n} + \phi_{s_2} \phi_{s_2 n}, \end{aligned} \quad (17)$$

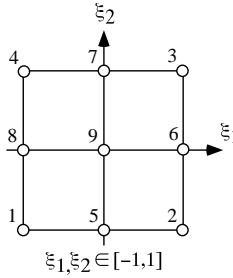
where s_1 and s_2 are local tangential coordinates on the body surface and k_1 and k_2 are curvature along s_1 and s_2 respectively.

2.3 DISCRETIZED BIE FOR NUMERICAL SOLUTION

2D element



3D rectangular element



3D triangular element

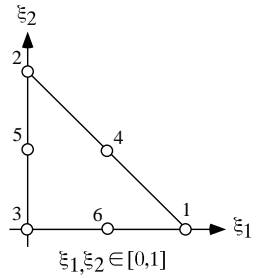


Fig.2 Quadratic elements used for 2D and 3D BEM

The boundary conditions are essentially nonlinear and the analytical solution of BIE is hardly obtained. To solve BIE numerically, boundary element method (BEM) is usually applied. In BEM, boundary S is divided into many small elements. On a element, the boundary shape and distribution of variables are approximated by polynomials of local coordinate. Constant approximation is the easiest but continuity of variables between adjacent elements is not guaranteed. At least, linear approximation is recommended. Generally in a element, the approximation of physical variable f is written as

$$\tilde{f} = \sum_j \sigma_j f_j, \quad (18)$$

where \tilde{f} is approximation function of f , f_j is a value of f at j th node of the element. Any variables such as ϕ , ϕ_n , ψ and boundary shape $\mathbf{x} = (x, y, z)$ can be substituted for f in above approximation. σ_j is so called shape function. For example, shape functions of quadratic element for 2D BEM are given as

$$\left. \begin{aligned} \sigma_1 &= \xi_1(\xi_1 - 1)/2 \\ \sigma_2 &= (1 - \xi_1^2) \\ \sigma_3 &= \xi_1(\xi_1 + 1)/2 \end{aligned} \right\} \quad (19)$$

and shape functions of quadratic 9 points rectangular element and quadratic triangular element for 3D BEM are respectively given as follows.

$$\left. \begin{aligned} \sigma_1 &= \xi_1\xi_2(\xi_1 - 1)(\xi_2 - 1)/4 \\ \sigma_2 &= \xi_1\xi_2(\xi_1 + 1)(\xi_2 - 1)/4 \\ \sigma_3 &= \xi_1\xi_2(\xi_1 + 1)(\xi_2 + 1)/4 \\ \sigma_4 &= \xi_1\xi_2(\xi_1 - 1)(\xi_2 + 1)/4 \\ \sigma_5 &= \xi_2(1 - \xi_1^2)(\xi_2 - 1)/2 \\ \sigma_6 &= \xi_1(1 - \xi_2^2)(\xi_1 + 1)/2 \\ \sigma_7 &= \xi_2(1 - \xi_1^2)(\xi_2 + 1)/2 \\ \sigma_8 &= \xi_1(1 - \xi_2^2)(\xi_1 - 1)/2 \\ \sigma_9 &= (1 - \xi_1^2)(1 - \xi_2^2) \end{aligned} \right\} \quad (20)$$

$$\left. \begin{aligned} \sigma_1 &= \xi_1(2\xi_1 - 1) \\ \sigma_2 &= \xi_2(2\xi_2 - 1) \\ \sigma_3 &= (1 - \xi_1 - \xi_2)(1 - 2\xi_1 - 2\xi_2) \\ \sigma_4 &= 4\xi_1\xi_2 \\ \sigma_5 &= 4\xi_2(1 - \xi_1 - \xi_2) \\ \sigma_6 &= 4\xi_1(1 - \xi_1 - \xi_2) \end{aligned} \right\} \quad (21)$$

Where ξ_1 and ξ_2 are normalized local coordinates of the elements, see Fig.2. These higher order elements are widely used. Using eq.(18), following discretized BIEs of eq.(2) and (6) are obtained,

$$\sum_{j=1}^N H_{ij}\phi_j = \sum_{j=1}^N G_{ij}\phi_{nj} \quad (22)$$

$$\sum_{j=1}^N H'_{ij}\phi_j = \sum_{j=1}^N G'_{ij}\psi_j, \quad (23)$$

where N is total number of collocation points, subscript i, j indicate the serial number of collocation point and matrices $H_{ij}, H'_{ij}, G_{ij}, G'_{ij}$ represent the influence of point P_i to point P_j . These matrices are usually called as influence matrices. The boundary integral on a element is carried out analytically or numerically. Gaussian numerical integration, Abramowitz and Stegun (1964), is accurate and popularly used for numerical integral.

These linear equations can be solved by appropriate matrix solver. For small scale computation, we can use non-iterative solver like Gaussian elimination method, L/U decomposition method, etc. These common matrix solvers are found in mathematical libraries available on many computer systems. For large scale computation, iterative solver is faster. Particularly in 3D simulation, number of collocation points usually exceeds 10 thousands and fast matrix solver is indispensable. When we use iterative solver, we have to be careful about the conditional number of the matrix. Iterative matrix solver with preconditioning such as generalized minimal residual method (GMRES) by Saad and Schultz (1985) is

one of the best choice. Explanation of GMRES is given by Barrett et al. (1994) and its efficiency for large dense nonsymmetric matrix is studied by Zou and Kim (1996).

2.4 INSTANTANEOUS FREE SURFACE MOTION

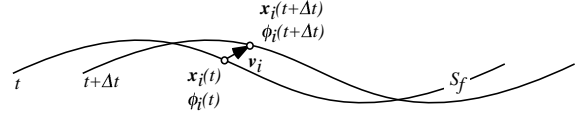


Fig.3 Mixed Eulerian and Lagrangian method

In this section, we pay attention to a point P on free surface. Here, the coordinate of P is denoted as $\mathbf{x}(P) = (x(P), y(P), z(P))$ and velocity potential at P is denoted as $\phi(P)$. Let us observe the time variation of $\mathbf{x}(P)$ and $\phi(P)$. Time derivative of $\mathbf{x}(P)$ and $\phi(P)$ are written as

$$\frac{d\mathbf{x}(P)}{dt} = \mathbf{v}(P) \quad (24)$$

$$\frac{d\phi(P)}{dt} = \phi_t + \mathbf{v}(P)\nabla\phi, \quad (25)$$

where $\mathbf{v}(P)$ is velocity of P .

First, we fix the point P to the fluid particle. This is so called Lagrangian method. Then, $\mathbf{v}(P)$ is equal to fluid velocity.

$$\mathbf{v}(P) = \nabla\phi \quad (26)$$

Substituting this equation and eq.(7) into eq.(25), we have

$$\frac{D\phi(P)}{Dt} = -z(P) + \frac{1}{2}\nabla\phi \cdot \nabla\phi. \quad (27)$$

Next, point P is fixed to free surface and allowed to move vertical direction only. In this semi-Lagrangian method, $\mathbf{v}(P)$ is given by

$$\mathbf{v}(P) = (0, 0, \phi_z) \quad (28)$$

Accordingly we have

$$\frac{d\phi(P)}{dt} = -z(P) - \frac{1}{2}(\phi_x^2 + \phi_y^2) + \frac{1}{2}\phi_z^2 \quad (29)$$

In 3D NWT, calculation of $\nabla\phi$ on free surface is a little troublesome. If higher order BEM is used, $\nabla\phi$ can be calculated in a panel by

$$\begin{Bmatrix} \phi_x \\ \phi_y \\ \phi_z \end{Bmatrix} = \begin{bmatrix} \frac{\partial x}{\partial \xi_1} & \frac{\partial y}{\partial \xi_1} & \frac{\partial z}{\partial \xi_1} \\ \frac{\partial x}{\partial \xi_2} & \frac{\partial y}{\partial \xi_2} & \frac{\partial z}{\partial \xi_2} \\ n_x & n_y & n_z \end{bmatrix}^{-1} \begin{Bmatrix} \phi_{\xi_1} \\ \phi_{\xi_2} \\ \phi_n \end{Bmatrix} \quad (30)$$

where ξ_1, ξ_2 is local coordinate of elements. However, even if higher order BEM is used, continuity of derivatives between adjacent panels are not always guaranteed. Then, $\nabla\phi$ is calculated by introducing a local higher order element which includes the boundary node P at the center. This element is independent of BEM and only used to calculate tangential derivatives at the center. If free surface panels are rectangle and have

lattice structure in real plane or mapping plane, spline fitting in both lattice directions is also a good method to calculate tangential derivatives of ϕ . Spline fitting are explained in §3.2.

Suppose the free surface profile, potential value on it and all other boundary conditions are given. We can use them as the initial condition of the simulation.

First, discretized BIE is solved.

Second, instantaneous motion of free surface particle is calculated by eq.(26) ~ (29).

Third, free surface is updated by

$$\mathbf{x}(P, t + \Delta t) = \mathbf{x}(P, t) + \int_t^{t+\Delta t} \mathbf{v}(P) dt \quad (31)$$

$$\phi(P, t + \Delta t) = \phi(P, t) + \int_t^{t+\Delta t} \frac{d\phi(P)}{dt} dt . \quad (32)$$

Fully nonlinear free surface motion can be simulated by this sequence. This method was developed by Longuet-Higgins & Cokelet (1976) and well known as Mixed Eulerian and Lagrangian (MEL) method. Since MEL method was originally developed to simulate plunging waves, eq.(26) and (27) were used in the original paper. Semi-Lagrangian method is widely used to simulate 3D wave diffraction problem by fixed bodies with vertical wall.

In practical codes, higher order time integral schemes are used for accurate and stable simulation. Time integral schemes are explained in §2.6.

2.5 INSTANTANEOUS FLOATING BODY MOTIONS

To calculate instantaneous floating body motions (i.e. velocity and acceleration of the floating body at each time step), we have to solve the simultaneous equation of fluid and floating body motions. The equation of ideal fluid motion (i.e. Euler's equation) is simply written as

$$\mathbf{a} = -\nabla(p + z) , \quad (33)$$

where p is pressure. Comparing this equation with eq.(10), Bernoulli's pressure equation is obtained.

$$p = -\phi_t - \frac{1}{2} \nabla \phi \cdot \nabla \phi - z \quad (34)$$

The second and the third term of right side of the equation can be evaluated from the solution of BIE with respect to ϕ . Calculation of these terms are explicit. On the other hand, the first term ϕ_t is obtained by solving the implicit loop of variables with concerning equations shown in Fig.4. Needless to say, equation of floating body motions is indispensable to determine ϕ_t . Solutions of this implicit loop were studied in the past two decades and following four consistent methods were developed.

- (1) Iterative method
- (2) Modal decomposition method
- (3) Indirect method
- (4) Implicit boundary condition method

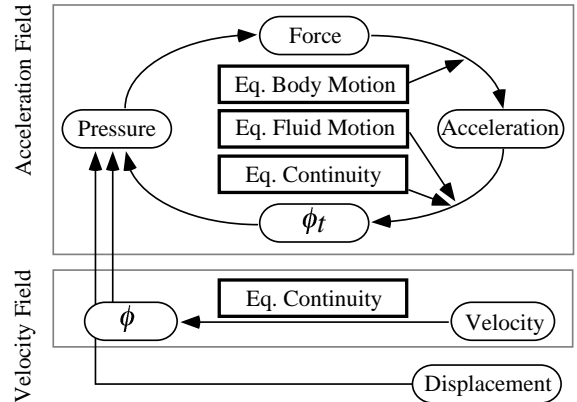


Fig.4 Loop structure of variables and concerning equations of acceleration field

2.5.1 Iterative method

Iterative method is the simplest. Started from an appropriate body acceleration at a guess, the loop of acceleration field is iteratively solved until the body acceleration converges to the steady value. Body acceleration of the last time step can be a good guess of initial value. This procedure has four steps. With the solution of ϕ and given initial body acceleration,

- 1) value of ϕ_{tn} on the body surface is calculated by eq.(13),
- 2) BIE with respect to ϕ_t is solved,
- 3) pressure distribution is calculated by eq.(34)
- 4) hydrodynamic force is obtained by pressure integration,
- 5) new body acceleration is obtained from equation of body motion,
- 6) Continue (1) to (5) until convergence.

Cao, Beck and Schultz (1994) used this method and showed that the convergence of this method is excellent. The simplicity of this method is a big merit for programming. However, since we have to solve BIE several times in a single time step, this method is time consuming. Sen (1993) also adopted iterative method to simulated rectangular body motions in regular waves. In his method, BIE of ϕ_t is not solved but approximated by finite difference.

2.5.2 Modal decomposition method

Modal decomposition method was developed by Vinje and Brevig (1981a,1981b). They developed two dimensional NWT based on complex potential. In their NWT, the acceleration field is decomposed into four modes corresponding to three unit accelerations of body motion (heave, sway and roll) and the acceleration due to velocity field. Using the solution of four independent BIE together with equation of body motions, body acceleration is determined. Cointe et al. (1990) also used modal decomposition method and developed linear and nonlinear 2D NWT based on velocity potential.

Let us look at a little detail of modal decomposition method for 3D problems. In this method, ϕ_t is

decomposed into 7 modes.

$$\phi_t = \sum_{j=1}^6 \alpha_j \varphi_j + \varphi_7, \quad (35)$$

where α_j is the j th mode component of the generalized acceleration of body. Comparing this equation with eq.(15), we can understand that φ_j , ($j = 1 \sim 6$) is corresponding to α_j and φ_7 is corresponding to q . Body surface boundary condition of each mode is

$$\varphi_{nj} = \begin{cases} N_j, & j = 1 \sim 6 \\ q, & j = 7. \end{cases} \quad (36)$$

On free surface, homogeneous boundary condition is applied to modes $j = 1 \sim 6$. The free surface boundary condition for each mode is written as

$$\varphi_j = \begin{cases} 0, & j = 1 \sim 6 \\ \frac{1}{2} \nabla \phi \cdot \nabla \phi + z, & j = 7. \end{cases} \quad (37)$$

Solving the above BIEs, φ_j , ($j = 1 \sim 7$) is obtained. Integral of φ_j on the body surface gives the hydrodynamic force F_{ij} of i th direction.

$$F_{ij} = \int_{S_b} -\varphi_j N_i dS \quad j = 1 \sim 7, \quad (38)$$

In addition to these hydrodynamic components, we have to take into account the following component.

$$F_{i8} = \int_{S_b} \left\{ -\frac{1}{2} \nabla \phi \cdot \nabla \phi - z \right\} N_i dS \quad (39)$$

This component can be explicitly calculated from body position and ϕ . Then, total hydrodynamic force F_i is given by

$$F_i = \sum_{j=1}^6 \alpha_j F_{ij} + F_{i7} + F_{i8}, \quad (40)$$

where unknown body acceleration α_j is still included. Equation of body motion can be used to solve α_j .

$$\sum_{j=1}^6 \mathcal{M}_{ij} \alpha_j + \beta_i = F_i + F_{gi}, \quad (41)$$

where \mathcal{M}_{ij} is inertia tensor of the body, β_i is so called Gyro-moment, F_{gi} is sum of other external forces like gravity, thrust, mooring force etc. Substituting this equation into eq.(40), α_j is determined.

2.5.3 Indirect method

In linear theory, we can use Haskind-Newman relation to calculate hydrodynamic force from the solution of radiation problem. Wu & Eatock Taylor (1996) introduced the same idea to solve acceleration field. Kashiwagi (1998) called this method as new indirect method and used in his NWT.

Since ϕ_t and φ_i ($i = 1 \sim 6$) defined in eq.(35) satisfy Laplace's equation, we can apply Green's theorem to have

$$\int_{S_b+S_f+S_\infty} \{\phi_t \varphi_{ni} - \varphi_i \phi_{tn}\} dS = 0 \quad (42)$$

where S_∞ is fixed wall or imaginary wall far from the body. On S_∞ , $\varphi_{ni} = 0$ and $\phi_{tn} = 0$ are imposed. Using eq.(36) and (37), hydrodynamic force can be evaluated by

$$\begin{aligned} \int_{S_b} \phi_t N_i dS &= \int_{S_b} \varphi_i \phi_{tn} dS - \int_{S_f} \phi_t \varphi_{ni} dS \\ &= \int_{S_b} \varphi_i \left\{ \sum_{j=1}^6 \alpha_j N_j + q \right\} dS \\ &\quad + \int_{S_f} \left\{ \frac{1}{2} \nabla \phi \cdot \nabla \phi + z \right\} \varphi_{ni} dS \end{aligned} \quad (43)$$

Eq.(15) on S_b and $p = 0$ on S_f is considered for the derivation of eq.(43). Components of hydrodynamic force are written as

$$F_{ij} = \int_{S_b} \varphi_i N_j dS = \int_{S_b} \varphi_j N_i dS \quad (44)$$

$$F_{7i} = - \int_{S_b} \varphi_i q dS - \int_{S_f} \left\{ \frac{1}{2} \nabla \phi \cdot \nabla \phi + z \right\} \varphi_{ni} dS. \quad (45)$$

Symmetrical relation in eq.(44) is easily proved by applying Green's theorem to φ_i and φ_j . Difference between modal decomposition method and indirect method is found in the evaluation of F_{7i} . In modal decomposition method, BIE of φ_7 have to be solved. However, in indirect method, eq.(45) does not include φ_7 and F_{7i} is evaluated from φ_i ($i = 1 \sim 6$) indirectly. As mentioned above, φ_i ($i = 1 \sim 6$) is independent on velocity field and can be solved with ϕ at the same time. Consequently, indirect method is effective to reduce CPU time considerably. However, since pressure distribution is not calculated, this method can not be used when we need pressure distribution. Procedure to solve unknown body acceleration is the same as that of modal decomposition method.

2.5.4 Implicit boundary condition method

Equation of body motion (41) can be written in matrix and vector form.

$$\mathcal{M} \boldsymbol{\alpha} + \boldsymbol{\beta} = \mathbf{F}_f + \mathbf{F}_g \quad (46)$$

This equation is called Euler's equation of rigid body motion. Using generalized normal vector of the body surface \mathbf{N} , generalized hydrodynamic force \mathbf{F}_f is given by following pressure integral.

$$\mathbf{F}_f = \int_{S_b} \left(-\phi_t - \frac{1}{2} \nabla \phi \cdot \nabla \phi - z \right) \mathbf{N} dS \quad (47)$$

Here, we can use eq.(46) and (47) to eliminate unknown body acceleration $\boldsymbol{\alpha}$ from eq.(15).

$$\phi_{tn} = \mathbf{N} \mathcal{M}^{-1} \left\{ \int_{S_b} -\phi_t \mathbf{N} dS \right\} + Q, \quad (48)$$

where Q is

$$\begin{aligned} Q &= \mathbf{N} \mathcal{M}^{-1} \left\{ \int_{S_b} \left(-z - \frac{1}{2} \nabla \phi \cdot \nabla \phi \right) \mathbf{N} dS \right. \\ &\quad \left. + \mathbf{F}_g - \boldsymbol{\beta} \right\} + q. \end{aligned} \quad (49)$$

Eq.(48) is the implicit boundary condition which relates ϕ_t and $\partial\phi_t/\partial n$ on wet surface of the floating body. Tanizawa (1990,1995) introduced this implicit boundary condition and derived discretized BIE combined with it.

BIE (22) with respect to ϕ_t is written in matrix form as

$$[\mathbf{H}]\{\phi_t\} = [\mathbf{G}]\{\phi_{tn}\}, \quad (50)$$

where $[\mathbf{H}]$ and $[\mathbf{G}]$ are square matrices of size N . In the implicit boundary condition method, integral in eq.(48) is also discretized by BEM as

$$\{\phi_{tn}\} = -[\mathbf{A}]\{\phi_t\} + \{Q\}, \quad (51)$$

where collocation points on wet body surface are serially numbered from n_{w1} to n_{w2} and $[\mathbf{A}]$ is square matrices of size $n_{w2} - n_{w1} + 1$. Extending the size of $[\mathbf{A}]$ and $\{\phi_{tn}\}$ to N as follows,

$$A'_{ij} = \begin{cases} A_{ij}, & i, j \in [n_{w1}, n_{w2}] \\ 0, & otherwise \end{cases}, \quad (52)$$

$$\phi'_{tn,j} = \begin{cases} Q_j, & j \in [n_{w1}, n_{w2}] \\ \phi_{tn,j}, & otherwise \end{cases}, \quad (53)$$

we can combine eq. (51) and (50) in a single equation

$$[\mathbf{H} + \mathbf{G}\mathbf{A}']\{\phi_t\} = [\mathbf{G}]\{\phi'_{tn}\}. \quad (54)$$

In this BIE, unknown body acceleration is not included. Therefore, BIE is solvable without any decomposition or iteration. Hydrodynamic pressure is obtained from the solution of this BIE, hydrodynamic forces are given by eq.(47) and body acceleration is given by eq.(46).

Tanizawa (1997a,1998) applied this method to simulate parametric and chaotic roll motions. Ikeno and Matsuyama (1996) used this method in their 2D NWT and simulated motions of moored floating structure in tsunami. Van Daalen (1993) also used same type of implicit condition in 2D NWT. Recently, Berkvens(1998), Ikeno(2000) and Shirakura (2000) used this method in their 3D-NWTs.

2.6 TIME INTEGRAL

For time domain simulation, time integral method is very important to keep its accuracy and stability. In many practical NWT, higher order time integral method is used such as 4th order Runge-Kutta method (RK), 5th order Runge-Kutta-Gil method (RKG) and 4th order Adams-Bashforth-Moulton method (ABM). RK has $\mathcal{O}(\Delta t^4)$ accuracy, RKG has $\mathcal{O}(\Delta t^5)$ accuracy for short time simulation but $\mathcal{O}(\Delta t^4)$ for long time simulation and ABM has $\mathcal{O}(\Delta t^4)$ accuracy. With use of these methods, ordinary waves and floating body motions can be simulated stably even for large time increment $\Delta t \leq T_w/20$, where T_w is wave period.

In this section, $\mathbf{x}_i(t), \phi_i(t)$ denote location and velocity potential of free surface node i , $\mathbf{R}(t), \mathbf{V}(t)$ denote position and velocity of floating body and $S(t) = S(\mathbf{x}_i(t), \mathbf{R}(t))$ denotes boundary shape. $\phi(S(t))$ and $\phi_t(S(t))$ denote solution of BIEs with respect to boundary shape $S(t)$ and $\boldsymbol{\alpha}(\phi(S(t)), \phi_t(S(t)))$ denotes the

acceleration of floating body as a function of $\phi(S(t))$ and $\phi_t(S(t))$.

In RK and RKG, following four steps are required to advance the simulation single time step Δt .

The first step

$$\left. \begin{aligned} \Delta \mathbf{x}_{i1} &= \Delta t \nabla \phi(S(t)) \\ \Delta \phi_{i1} &= \Delta t(-z_i(t) + \frac{1}{2}(\nabla \phi(S(t)))^2) \\ \Delta \mathbf{V}_1 &= \Delta t \boldsymbol{\alpha}(\phi(S(t)), \phi_t(S(t))) \\ \Delta \mathbf{R}_1 &= \Delta t \mathbf{V}(t) \\ \mathbf{x}_{i1} &= \mathbf{x}_i(t) + \frac{1}{2} \Delta \mathbf{x}_{i1} \\ \phi_{i1} &= \phi_i(t) + \frac{1}{2} \Delta \phi_{i1} \\ \mathbf{V}_1 &= \mathbf{V}(t) + \frac{1}{2} \Delta \mathbf{V}_1 \\ \mathbf{R}_1 &= \mathbf{R}(t) + \frac{1}{2} \Delta \mathbf{R}_1 \\ S_1 &= S(\mathbf{x}_{i1}, \mathbf{R}_1) \\ \phi(S_1) &\Leftarrow B.E.M. \\ \phi_t(S_1) &\Leftarrow B.E.M. \end{aligned} \right\} \quad (55)$$

The second step

$$\left. \begin{aligned} \Delta \mathbf{x}_{i2} &= \Delta t \nabla \phi(S_1) \\ \Delta \phi_2 &= \Delta t(-z_{i1} + \frac{1}{2}(\nabla \phi(S_1))^2) \\ \Delta \mathbf{V}_2 &= \Delta t \boldsymbol{\alpha}(\phi(S_1), \phi_t(S_1)) \\ \Delta \mathbf{R}_2 &= \Delta t \mathbf{V}_1 \\ \mathbf{x}_{i2} &= \mathbf{x}_i(t) + c_1 \Delta \mathbf{x}_{i1} + c_2 \Delta \mathbf{x}_{i2} \\ \phi_{i2} &= \phi_i(t) + c_1 \Delta \phi_{i1} + c_2 \Delta \phi_{i2} \\ \mathbf{V}_2 &= \mathbf{V}(t) + c_1 \Delta \mathbf{V}_1 + c_2 \Delta \mathbf{V}_2 \\ \mathbf{R}_2 &= \mathbf{R}(t) + c_1 \Delta \mathbf{R}_1 + c_2 \Delta \mathbf{R}_2 \\ S_2 &= S(\mathbf{x}_{i2}, \mathbf{R}_2) \\ \phi(S_2) &\Leftarrow B.E.M. \\ \phi_t(S_2) &\Leftarrow B.E.M. \end{aligned} \right\} \quad (56)$$

The third step

$$\left. \begin{aligned} \Delta \mathbf{x}_{i3} &= \Delta t \nabla \phi(S_2) \\ \Delta \phi_3 &= \Delta t(-z_{i2} + \frac{1}{2}(\nabla \phi(S_2))^2) \\ \Delta \mathbf{V}_3 &= \Delta t \boldsymbol{\alpha}(\phi(S_2), \phi_t(S_2)) \\ \Delta \mathbf{R}_3 &= \Delta t \mathbf{V}_2 \\ \mathbf{x}_{i3} &= \mathbf{x}_i(t) + c_3 \Delta \mathbf{x}_{i2} + c_4 \Delta \mathbf{x}_{i3} \\ \phi_{i3} &= \phi_i(t) + c_3 \Delta \phi_{i2} + c_4 \Delta \phi_{i3} \\ \mathbf{V}_3 &= \mathbf{V}(t) + c_3 \Delta \mathbf{V}_2 + c_4 \Delta \mathbf{V}_3 \\ \mathbf{R}_3 &= \mathbf{R}(t) + c_3 \Delta \mathbf{R}_2 + c_4 \Delta \mathbf{R}_3 \\ S_3 &= S(\mathbf{x}_{i3}, \mathbf{R}_3) \\ \phi(S_3) &\Leftarrow B.E.M. \\ \phi_t(S_3) &\Leftarrow B.E.M. \end{aligned} \right\} \quad (57)$$

The fourth step

$$\left. \begin{aligned} \Delta \mathbf{x}_{i4} &= \Delta t \nabla \phi(S_3) \\ \Delta \phi_4 &= \Delta t(-z_{i3} + \frac{1}{2}(\nabla \phi(S_3))^2) \\ \Delta \mathbf{V}_4 &= \Delta t \boldsymbol{\alpha}(\phi(S_3), \phi_t(S_3)) \\ \Delta \mathbf{R}_4 &= \Delta t \mathbf{V}_3 \\ \mathbf{x}_i(t + \Delta t) &= \mathbf{x}_i(t) + \frac{1}{6} \{\Delta \mathbf{x}_{i1} + c_5 \Delta \mathbf{x}_{i2} \\ &\quad + c_6 \Delta \mathbf{x}_{i3} + \Delta \mathbf{x}_{i4}\} \\ \phi_i(t + \Delta t) &= \phi_i(t) + \frac{1}{6} \{\Delta \phi_1 + c_5 \Delta \phi_2 \\ &\quad + c_6 \Delta \phi_3 + \Delta \phi_4\} \\ \mathbf{V}(t + \Delta t) &= \mathbf{V}(t) + \frac{1}{6} \{\Delta \mathbf{V}_1 + c_5 \Delta \mathbf{V}_2 \\ &\quad + c_6 \Delta \mathbf{V}_3 + \Delta \mathbf{V}_4\} \\ \mathbf{R}(t + \Delta t) &= \mathbf{R}(t) + \frac{1}{6} \{\Delta \mathbf{R}_1 + c_5 \Delta \mathbf{R}_2 \\ &\quad + c_6 \Delta \mathbf{R}_3 + \Delta \mathbf{R}_4\} \\ S(t + \Delta t) &= S(\mathbf{x}_i(t + \Delta t), \mathbf{R}(t + \Delta t)) \\ \phi(S(t + \Delta t)) &\Leftarrow B.E.M. \\ \phi_t(S(t + \Delta t)) &\Leftarrow B.E.M. \end{aligned} \right\} \quad (58)$$

Coefficients $c_1 \sim c_6$ are given in the following table.

Coefficient	RK	RKG
c_1	0	$(\sqrt{2} - 1)/2$
c_2	1/2	$(2 - \sqrt{2})/2$
c_3	0	$-\sqrt{2}/2$
c_4	1	$(2 + \sqrt{2})/2$
c_5	2	$2 - \sqrt{2}$
c_6	2	$2 + \sqrt{2}$

ABM is a predictor-corrector method and following two steps are required to advance the simulation single time step.

The first prediction step

$$\left. \begin{aligned}
\Delta \mathbf{x}_i(t) &= \Delta t \nabla \phi(S(t)) \\
\Delta \phi_i(t) &= \Delta t (-z_i(t) + \frac{1}{2} (\nabla \phi(S(t)))^2) \\
\Delta \mathbf{V}(t) &= \Delta t \boldsymbol{\alpha}(\phi(S(t)), \phi_t(S(t))) \\
\Delta \mathbf{R}(t) &= \Delta t \mathbf{V}(t) \\
\mathbf{x}_i(t + \Delta t) &= \mathbf{x}_i(t) + \frac{1}{24} \{ 55 \Delta \mathbf{x}_i(t) \\
&\quad - 59 \Delta \mathbf{x}_i(t - \Delta t) \\
&\quad + 37 \Delta \mathbf{x}_i(t - 2\Delta t) \\
&\quad - 9 \Delta \mathbf{x}_i(t - 3\Delta t) \} \\
\phi_i(t + \Delta t) &= \phi_i(t) + \frac{1}{24} \{ 55 \Delta \phi_i(t) \\
&\quad - 59 \Delta \phi_i(t - \Delta t) \\
&\quad + 37 \Delta \phi_i(t - 2\Delta t) \\
&\quad - 9 \Delta \phi_i(t - 3\Delta t) \} \\
\mathbf{V}(t + \Delta t) &= \mathbf{V}(t) + \frac{1}{24} \{ 55 \Delta \mathbf{V}(t) \\
&\quad - 59 \Delta \mathbf{V}(t - \Delta t) \\
&\quad + 37 \Delta \mathbf{V}(t - 2\Delta t) \\
&\quad - 9 \Delta \mathbf{V}(t - 3\Delta t) \} \\
\mathbf{R}(t + \Delta t) &= \mathbf{R}(t) + \frac{1}{24} \{ 55 \Delta \mathbf{R}(t) \\
&\quad - 59 \Delta \mathbf{R}(t - \Delta t) \\
&\quad + 37 \Delta \mathbf{R}(t - 2\Delta t) \\
&\quad - 9 \Delta \mathbf{R}(t - 3\Delta t) \} \\
S(t + \Delta t) &= S(\mathbf{x}_i(t + \Delta t), \mathbf{R}(t + \Delta t)) \\
\phi(S(t + \Delta t)) &\Leftarrow B.E.M. \\
\phi_t(S(t + \Delta t)) &\Leftarrow B.E.M.
\end{aligned} \right\} \quad (59)$$

The second correction step

$$\left. \begin{aligned}
\Delta \mathbf{x}_i(t + \Delta t) &= \Delta t \nabla \phi(S(t + \Delta t)) \\
\Delta \phi_i(t + \Delta t) &= \Delta t (-z_i(t + \Delta t) \\
&\quad + \frac{1}{2} (\nabla \phi(S(t + \Delta t)))^2) \\
\Delta \mathbf{V}(t + \Delta t) &= \Delta t \boldsymbol{\alpha}(\phi(S(t + \Delta t)), \phi_t(S(t + \Delta t))) \\
\Delta \mathbf{R}(t + \Delta t) &= \Delta t \mathbf{V}(t + \Delta t) \\
\mathbf{x}_i(t + \Delta t) &= \mathbf{x}_i(t) + \frac{1}{24} \{ 9 \Delta \mathbf{x}_i(t + \Delta t) \\
&\quad + 19 \Delta \mathbf{x}_i(t) \\
&\quad - 5 \Delta \mathbf{x}_i(t - \Delta t) \\
&\quad + \Delta \mathbf{x}_i(t - 2\Delta t) \} \\
\phi_i(t + \Delta t) &= \phi_i(t) + \frac{1}{24} \{ 9 \Delta \phi_i(t + \Delta t) \\
&\quad + 19 \Delta \phi_i(t) \\
&\quad - 5 \Delta \phi_i(t - \Delta t) \\
&\quad + \Delta \phi_i(t - 2\Delta t) \} \\
\mathbf{V}(t + \Delta t) &= \mathbf{V}(t) + \frac{1}{24} \{ 9 \Delta \mathbf{V}(t + \Delta t) \\
&\quad + 19 \Delta \mathbf{V}(t) \\
&\quad - 5 \Delta \mathbf{V}(t - \Delta t) \\
&\quad + \Delta \mathbf{V}(t - 2\Delta t) \} \\
\mathbf{R}(t + \Delta t) &= \mathbf{R}(t) + \frac{1}{24} \{ 9 \Delta \mathbf{R}(t + \Delta t) \\
&\quad + 19 \Delta \mathbf{R}(t) \\
&\quad - 5 \Delta \mathbf{R}(t - \Delta t) \\
&\quad + \Delta \mathbf{R}(t - 2\Delta t) \} \\
S(t + \Delta t) &= S(\mathbf{x}_i(t + \Delta t), \mathbf{R}(t + \Delta t)) \\
\phi(S(t + \Delta t)) &\Leftarrow B.E.M. \\
\phi_t(S(t + \Delta t)) &\Leftarrow B.E.M.
\end{aligned} \right\} \quad (60)$$

In RK and RKG, past record is unnecessary. Therefore, simulation can be started only with given initial condition. On the other hand, ABM requires record of past three steps. This is a disadvantage of ABM. However, ABM requires only two steps whereas RK and RKG require four time steps. Accordingly, simulation speed of ABM is double of that of RK and RKG. Dommermuth et al. (1988) combined RK and ABM. In their NWT, the first three time steps are simulate by RK and following steps are simulated by ABM until rearrangement of free surface collocation points. After the rearrangement, RK is used again to initiate simulation.

2.7 STABILITY ANALYSIS

Stability of NWT is closely related with time integral method. Dommermuth and Yue (1987) performed a von Neumann stability analysis for RK with linearized free surface boundary condition and obtained the Courant condition

$$\Delta t^2 \leq \frac{8}{\pi} \frac{\Delta x}{g}, \quad (61)$$

where Δx is local grid spacing. Dommermuth et al. (1988) also performed the same analysis for ABM and found that ABM is weakly unstable with growth rate proportional to $\Delta t^6 / \Delta x^3$. Based on these analysis, they introduced adaptive time increment procedure in their NWT for a plunging wave simulation. Since the Δt is so controlled as to satisfy the local Courant condition (61), Δt is variable. ABM can not be applied with variable Δt .

2.8 ACCURACY CHECK

Conservation check of fluid volume, momentum and energy is the most basic and widely used method to evaluate accuracy of simulations by NWT. To check the conservation laws, following items are computed during the simulation.

$$V_f = \int_{\Omega} dv = \int_S z n_z ds, \quad (62)$$

$$\mathbf{P}_f = \int_{\Omega} \nabla \phi dv = \int_S \phi \mathbf{n} ds, \quad (63)$$

$$\begin{aligned}
E_f &= \int_{\Omega} z + \frac{1}{2} \nabla \phi \cdot \nabla \phi dv \\
&= \frac{1}{2} \int_S -z^2 n_z + \phi \phi_n ds, \quad (64)
\end{aligned}$$

$$\mathbf{I} = \int_0^t \int_S p \mathbf{n} ds dt, \quad (65)$$

$$W = \int_0^t \int_S p \phi_n ds dt, \quad (66)$$

where V_f , \mathbf{P}_f and E_f are volume, momentum and energy of fluid respectively and \mathbf{I} and W are impulse and work given to fluid from the boundary.

Volume conservation is the most fundamental item to be checked. If BIE is accurately solved and MEL

method is correctly implemented, NWT satisfies volume conservation precisely.

Momentum and energy conservation are sensitive to the solution of ϕ_t . As eq.(63) ~ (66) show, Momentum \mathbf{P}_f and energy E_f are calculated from ϕ . On the other hand, impulse \mathbf{I} and work W are calculated from pressure p which is a function of both ϕ and ϕ_t . Errors of momentum E_m and energy E_e are respectively given as

$$E_m^2 = \int_0^T (\mathbf{P}_f(t) - \mathbf{I}(t))^2 dt / \int_0^T \mathbf{P}_f(t)^2 dt \quad (67)$$

$$E_e^2 = \int_0^T (E_f(t) - W(t))^2 dt / \int_0^T E_f(t)^2 dt. \quad (68)$$

Unless BIE with respect to ϕ_t is accurately solved, conservation laws are hard to be satisfied. In particular, for simulations of floating body motions, the loop of ϕ_t shown in Fig.4 must be solved by consistent methods such as presented in §2.5.

3 NUMERICAL TECHNIQUE

3.1 TREATMENT OF INTERSECTION

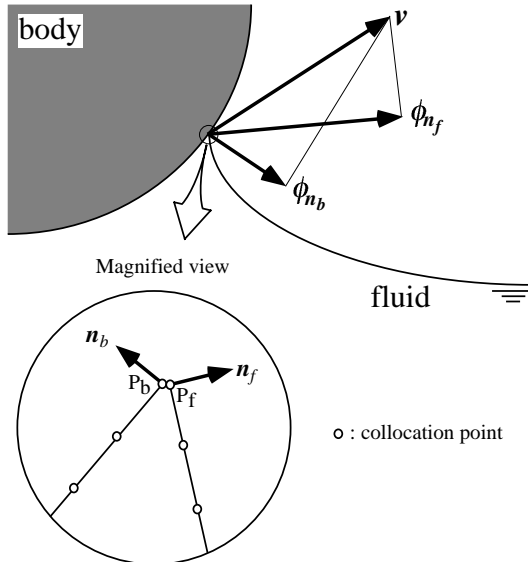


Fig.5 Magnified view of intersection

At the intersection of body surface and free surface, we have to take care of discontinuity of flux and singularity.

Discontinuity of flux is due to the discontinuity of normal direction at the intersection. To deal with this discontinuity, double node technique is popularly used. Fig.5 shows the intersection of 2D NWT. P_f and P_b are double nodes collocated at the same position, $\mathbf{n}_f = (n_{fx}, n_{fz})$ is unit normal vector of free surface and $\mathbf{n}_b = (n_{bx}, n_{bz})$ is that of body surface. Since the intersection is a vertex, \mathbf{n}_f and \mathbf{n}_b point different directions and so flux is discontinuous there. On the other hand, velocity potential is continuous. Value of $\phi(P_f)$ is given on free surface and value of $\phi_n(P_b)$ is given on body surface. Unknown $\phi_n(P_f)$ is obtained as a solution of BIE. Using double nodes, discontinuous flux at the intersection can be appropriately treated.

In linear theory, the intersection has $\mathcal{O}(\log r)$ singularity. Also in NWT, the intersection has weak singularity and the numerical treatment is one of the important issues. When we use NWTs, we sometimes encounter stability problem at the intersection. This instability is due to the accuracy of fluid velocity calculation at the intersection. In many NWTs, the velocity of the intersection is calculated from $\phi_n(P_b)$ and $\phi_s(P_b)$ on the body surface, where $\phi_s(P_b)$ is tangential derivative of ϕ calculated from the distribution of ϕ on the body surface boundary element. However, it is known that the convergence of $\phi_s(P_b)$ with respect to the size of boundary element is bad. Smaller element sometimes gives us higher ϕ_s . For accurate and stable simulation, tracking of intersection points must be as accurate as other points. In Fig.5, $\mathbf{v} = (v_x, v_z)$ is velocity of the fluid particle at the intersection. To calculate \mathbf{v} , we can use following relations.

$$\left. \begin{aligned} \phi_n(P_f) &= \mathbf{v} \cdot \mathbf{n}_f = v_x n_{fx} + v_z n_{fz} \\ \phi_n(P_b) &= \mathbf{v} \cdot \mathbf{n}_b = v_x n_{bx} + v_z n_{bz} \end{aligned} \right\}, \quad (69)$$

where \mathbf{n}_f and \mathbf{n}_b are obtained from the shape of the boundary. Using these relations, we can solve v_x and v_z . Tanizawa (1997b) reported that the velocity of the intersection calculated by this method is insensitive to the size of boundary element and simulated free surface near the intersection is stable and smooth.

Application of this method to 3D NWT is straight. Let us imagine the intersection line of free surface and body surface. In addition to \mathbf{n}_f and \mathbf{n}_b , tangential direction to the line \mathbf{s} have to be considered. Since the distribution of ϕ on the line is known, tangential derivative ϕ_s is also known. Similar to 2D case, double nodes P_f and P_b are collocated on the line and BIE is solved. Then, ϕ_{n_f} is obtained. The velocity on the intersection line $\mathbf{v} = (v_x, v_y, v_z)$ is calculated from

$$\left. \begin{aligned} \phi_n(P_f) &= \mathbf{v} \cdot \mathbf{n}_f \\ \phi_n(P_b) &= \mathbf{v} \cdot \mathbf{n}_b \\ \phi_s &= \mathbf{v} \cdot \mathbf{s} \end{aligned} \right\}. \quad (70)$$

Next, let us imagine the intersection point of free surface and two body surfaces such as a corner of 3D NWT. We need to use triple nodes technique to deal with three different normal direction. One is normal direction to free surface \mathbf{n}_f and the others are normal directions to two body surface \mathbf{n}_{b_1} and \mathbf{n}_{b_2} . At the intersection point, three points, P_f on free surface and P_{b_1} and P_{b_2} on the body surfaces, are collocated, BIE is solved and ϕ_{n_f} is obtained as the solution. The velocity at the intersection point is calculated from

$$\left. \begin{aligned} \phi_{n_f} &= \mathbf{v} \cdot \mathbf{n}_f \\ \phi_{n_{b_1}} &= \mathbf{v} \cdot \mathbf{n}_{b_1} \\ \phi_{n_{b_2}} &= \mathbf{v} \cdot \mathbf{n}_{b_2} \end{aligned} \right\}. \quad (71)$$

3.2 CURVE AND SURFACE FITTING BY SPLINE

Curve and surface fitting is indispensable to calculate tangential derivatives of variables on the boundary

surface. As eq.(16) and (17) show, the second derivatives are necessary to solve ϕ_t . Therefore, fitting function must be class C^n : $n \geq 2$. Curve and surface fitting is also indispensable for rearrangement of collocation points.

3.2.1 Fitting by cubic-B spline

Cubic-B spline is typical interpolation function generally used for curve fitting in 2D NWTs. Here, curve fitting of given sample points $\{f\} = \{f(x_1), f(x_2), \dots, f(x_n)\}^T$ of a single valued function $f(x)$ is considered. The proposition of curve fitting is obtaining the approximation function $\tilde{f}(x) \approx f(x)$ from the given sample points. In cubic-B spline interpolation method, $\tilde{f}(x)$ is expressed as the summation of piecewise cubic tent functions.

$$\tilde{f}(x) = \sum_{i=-1}^{n+2} w_i B_i(x), \quad (72)$$

where $B_i(x)$ is the piecewise cubic-B tent function and w_i is spline coefficient.

$$B_i(x) = \begin{cases} 0 & x < x_{i-2} \\ b_{1i}(x) & x_{i-2} \leq x < x_{i-1} \\ b_{2i}(x) & x_{i-1} \leq x < x_i \\ b_{3i}(x) & x_i \leq x < x_{i+1} \\ b_{4i}(x) & x_{i+1} \leq x < x_{i+2} \\ 0 & x_{i+2} \leq x \end{cases}$$

$$b_{1i}(x) = \frac{(x - x_{i-2})^3}{(x_{i+1} - x_{i-2})(x_i - x_{i-2})(x_{i-1} - x_{i-2})}$$

$$b_{2i}(x) = \frac{(x - x_{i-2})}{(x_{i+1} - x_{i-2})} \left\{ \frac{(x - x_{i-2})(x_i - x)}{(x_i - x_{i-2})(x_i - x_{i-1})} + \frac{(x_{i+1} - x)(x - x_{i-1})}{(x_{i+1} - x_{i-1})(x_i - x_{i-1})} \right\} + \frac{(x_{i+2} - x)(x - x_{i-1})^2}{(x_{i+2} - x_{i-1})(x_{i+1} - x_{i-1})(x_i - x_{i-1})}$$

$$b_{3i}(x) = \frac{(x_{i+2} - x)}{(x_{i+2} - x_{i-1})} \left\{ \frac{(x - x_{i-1})(x_{i+1} - x)}{(x_{i+1} - x_{i-1})(x_{i+1} - x_i)} + \frac{(x_{i+2} - x)(x - x_i)}{(x_{i+2} - x_i)(x_{i+1} - x_i)} \right\} + \frac{(x - x_{i-2})(x_{i+1} - x)^2}{(x_{i+1} - x_{i-2})(x_{i+1} - x_{i-1})(x_{i+1} - x_i)}$$

$$b_{4i}(x) = \frac{(x_{i+2} - x)^3}{(x_{i+2} - x_{i-1})(x_{i+2} - x_i)(x_{i+2} - x_{i+1})} \quad (73)$$

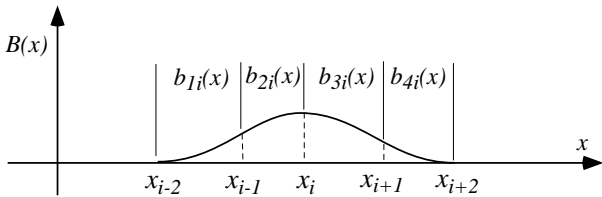


Fig.6 Cubic-B spline tent function

Substituting the sampling data $(x_i, f(x_i))$, $i = 1 \sim n$ and appropriate boundary condition at both sides of

sampling interval $(x_i, f(x_i))$, $i = -1, 0, n+1, n+2$ into eq.(72), a set of linear equation is obtained,

$$\{f\} = [S]\{w\}, \quad (74)$$

where $[S]$ is a penta-diagonal spline matrix. Spline coefficient $\{w\}$ is obtained by solving eq.(74),

$$\{w\} = [S]^{-1}\{f\}. \quad (75)$$

We can apply cubic-B spline to interpolate many-valued function such as plunging wave shape. Parameter expression of many-valued function $x = x(s), z = z(s)$ is used for interpolation. Curve-linear coordinate along the boundary is usually used for the parameter s . Since $x = x(s)$ and $z = z(s)$ are single valued functions, we can apply cubic-B spline to $x(s)$ and $z(s)$ individually.

Cubic-B spline is also used to interpolate 3D surface. If all panels are rectangle and have lattice structure in real plane or mapping plane, boundary value is expressed as a function of grid lines x and y . Thus boundary value are approximated by fitting function,

$$\tilde{f}(x, y) = \sum_{i=-1}^{n+2} \sum_{j=-1}^{m+2} w_{ij} B_i(x) B_j(y). \quad (76)$$

Spline coefficient w_{ij} is determined from sampling data $\{f(x_i, y_j)\}$, $i = 1 \sim n, j = 1 \sim m$.

3.2.2 Fitting by smoothing spline

Simulation of steep water waves sometimes break down from a point where a small scale wave breaking occurs. In many cases, such a unstable place and time is difficult to anticipate and so smoothing is applied to entire free surface through all time steps. However, smoothing is a error source and should not be used without evaluating its effect quantitatively. For practical use, weighted 3-points or 5-points smoothing are simple and easy to apply. For example, Longuet-Higgins and Cokelet (1976) tried following two 5-points smoothing formulae to remove saw-tooth instability.

$$\left. \begin{aligned} \bar{f}_j &= \frac{1}{16}(-f_{j-2} + 4f_{j-1} + 10f_j + 4f_{j+1} - f_{j+2}) \\ \bar{f}_j &= \frac{1}{32}(-f_{j-3} + 9f_{j-1} + 16f_j + 9f_{j+1} - f_{j+3}) \end{aligned} \right\} \quad (77)$$

Characteristic of these smoothing method is clear when arrangement of collocation points is uniform. If the arrangement is not uniform, neither is the smoothing effect. Smoothing methods based on FFT and inverse FFT are also applicable only to the uniform arrangement.

Ideal smoothing function for NWT should be applicable to irregular arrangement of collocation points. Its smoothing effect should be insensitive to the arrangement and controllable by specified wave number. To meet these requirement, smoothing spline is a good choice. Smoothing spline is a cubic spline function with smoothing effect. Characteristic of smoothing spline was studied by Craven and Wahba (1977) and Wahba (1981) and its basis was explained by Lancaster (1986).

Similar to cubic-B spline, we can use smoothing spline as higher order element of BEM. The characteristic smoothing spline can be analyzed as follows.

Again, interpolation of given sample points $\{f\} = \{f(x_1), f(x_2), \dots, f(x_n)\}^T$ of a single valued function $f(x)$ is considered. We need to find a piecewise cubic fitting function $\tilde{f}(x)$. Arrangement of x_i is not necessary uniform. Cubic-B spline interpolation function is bind to satisfy the condition $\tilde{f}(x_i) = f(x_i)$. On the other hand, smoothing spline is relaxed to satisfy this condition, but subject to minimize the functional K ,

$$K = J(f) + k_c^4 E(f) \quad (78)$$

$$J(f) = \int_{x_1}^{x_n} [\tilde{f}''(x)]^2 dx \quad (79)$$

$$E(f) = \int_{x_1}^{x_n} [\tilde{f}(x) - f(x)]^2 dx, \quad (80)$$

where $J(f)$ is strain energy of the spline function, $E(f)$ is square of fitting error and k_c is the parameter to specify the cutoff wave number of smoothing spline.

Fourier expansion of $f(x)$ and $\tilde{f}(x)$ are written as

$$f(x) = \sum_{j=0}^{\infty} f_j = \sum_{j=0}^{\infty} c_j e^{ik_j x} \quad (81)$$

$$\tilde{f}(x) = \sum_{j=0}^{\infty} \tilde{f}_j = \sum_{j=0}^{\infty} g_j c_j e^{ik_j x}, \quad (82)$$

where c_j and k_j are amplitude and wave number of j th component respectively and g_j is damping coefficient of j th component by smoothing spline. Substituting eq.(81) and (82) into (78), functional K is written as

$$K = \int_{x_1}^{x_n} \left[\sum_{j=0}^{\infty} (-k_j^2) g_j c_j e^{ik_j x} \right]^2 dx + \int_{x_1}^{x_n} \left[\sum_{j=0}^{\infty} k_c^2 (g_j - 1) c_j e^{ik_j x} \right]^2 dx. \quad (83)$$

Since $e^{ik_j x}$ is orthogonal function, eq.(83) can be simplified as

$$K = \sum_{j=0}^{\infty} K_j = \sum_{j=0}^{\infty} \int_{x_1}^{x_n} c_j^2 \{k_j^4 g_j^2 + k_c^4 (g_j - 1)^2\} e^{2ik_j x} dx, \quad (84)$$

where, the interval of the integral $[x_1 \leq x \leq x_n]$ is assumed to be much longer than wave length. Necessary condition to minimize the functional K is

$$\frac{\partial K_j}{\partial g_j} = 0. \quad (85)$$

Substituting eq.(84) into this condition, we have

$$k_j^4 g_j + k_c^4 (g_j - 1) = 0, \quad (86)$$

then damping ratio of j th component g_j is given as

$$g_j = \frac{1}{1 + (k_j/k_c)^4}. \quad (87)$$

Log scale plot of g_j is shown in Fig.7. For $k_j < k_c$, $g_j \approx 1$ and no smoothing take effects. On the other hand, for $k_j > k_c$, smoothing effect is remarkable. At $k_j/k_c = 10$, value of g_j becomes approximately $1/10000$. Therefore, this wave component will be totally cut off. Smoothing spline is a numerical low-pass filter at the same time spline interpolation function. Using parameter k_c , we can control the cutoff wave number of smoothing spline to remove unnecessary wave components.

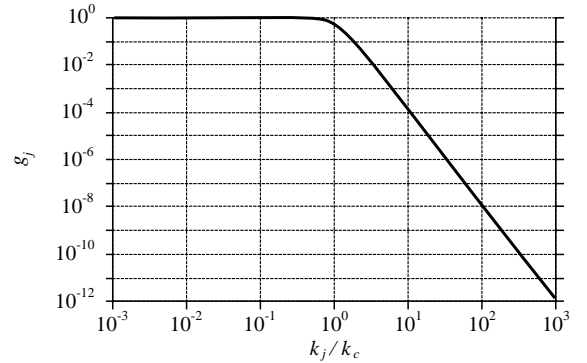


Fig.7 Characteristic of smoothing spline as a low pass filter

3.2.3 Fitting by spline-surface

Let us consider a function $f = f(x, y)$ of class C^n : $n \geq 2$. On the $x - y$ plane, sample points $P_i, i \dots n$ are randomly distributed and only the values at that points $f_i = f(P_i)$ are given. The proposition is obtaining the approximation function $\tilde{f}(x, y)$ of class C^2 . If points were regularly arranged on lattice, we could use cubic-B spline and $\tilde{f}(x, y)$ could be given by eq.(76). For randomly distributed points, cubic spline-surface is given by superposition of basis function as

$$\tilde{f}(x, y) = a + bx + cy + \sum_{i=1}^N w_i \beta(x - x_i, y - y_i), \quad (88)$$

where $\beta(x, y)$ is basis function and a, b, c, w_i are spline coefficients determined from sample points, Lancaster (1986). The simplest cubic basis function is

$$\beta(x, y) = \sqrt{x^2 + y^2}^3. \quad (89)$$

3.3 REARRANGEMENT OF COLLOCATION POINTS

For the stable simulation of free surface motion by MEL, rearrangement of collocation points is indispensable. The rearrangement is also necessary on the body surface because wet surface moves every time step with relative motion of free surface and body. The rearrangement is executed every time step on the body surface and every several time steps on the free surface. In

NWT codes, rearrangement is executed in succession of the curve and surface fitting. The collocation points are uniformly distributed in simplest rearrangement. However, it's desirable that rearrangement function has density control of collocation points. The density control on a curve and surface is explained in the following subsections.

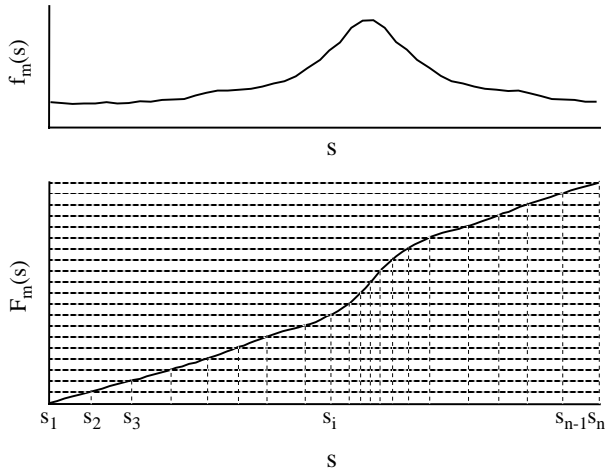


Fig.8 Mesh function and its integral

3.3.1 Density control on a curve

Hyman and Naughton (1985) introduced mesh function and developed a technique to control distribution of collocation points on a curve. This technique is useful for the rearrangement. First, let us introduce curvilinear coordinate s along a boundary and define a mesh function $f_m(s)$. Mesh function must be positive definite function. For example,

$$f_m(s) = \frac{|k(s)| + k_b}{|k_{max}| + k_b} \quad (90)$$

$$F_m(s) = \int_{s_1}^s f_m(s) ds, \quad (91)$$

where $k(s)$ is curvature of the boundary, k_{max} is its maximum value and k_b is positive parameter to control the ratio between maximum and minimum mesh sizes. $F_m(s)$ is the integral of the mesh function and monotone increasing. Fig.8 shows an example of $f_m(s)$ and $F_m(s)$. The arrangement of collocation points s_1, s_2, \dots, s_n are solved so as to satisfy the condition,

$$\Delta F_m = \int_{s_i}^{s_{i+1}} f_m(s) ds = \frac{F_m(s_n)}{n-1}. \quad (92)$$

This condition request that the integral of the mesh function on each boundary element is equal. The location of point i is given by the inverse function of $F_m(s)$ as

$$s_i = s_1 + F_m^{-1}(\Delta F_m(i-1)). \quad (93)$$

The mesh function (90) is simple but nicely works for the rearrangement of both free surface and body surface collocation points. In Fig.10, arrangement of collocation points by this mesh function is plotted as an example. If

more sophisticated control is necessary, various boundary values (*ex.* curvature, velocity, potential, flux etc.) can be used to define the mesh function.

Numerical error due to the interpolation and rearrangement is argued sometimes. However, this error is usually negligible because boundary element itself is a interpolation function, too. As far as the order of boundary element and interpolation function is the same, theoretically no error is born.

3.3.2 Density control on a surface

A closed area surrounded by boundary S is considered in $x-y$ plane. Uniform distribution of points P_i , $i = 1 \dots N$ inside and on the boundary S is the proposition. The points should be distributed as uniform as possible under the control of positive definite continuous function $d(x, y)$. $d(x, y)$ is so called density control function. Tanizawa (1995b) introduced following repulsion model. Denoting the position vector of point P_i as $\mathbf{r}_i = (x_i, y_i)$ and relative vector from P_i to P_j as $\mathbf{r}_{ij} = (x_i - x_j, y_i - y_j)$, repulsive force act to P_i from P_j is given as

$$\mathbf{f}_{ij} = \frac{\mathbf{r}_{ij}}{d_{ij} |\mathbf{r}_{ij}|^{n+1}}, \quad (94)$$

where $d_{ij} = d(x_i, y_i) d(x_j, y_j)$. This repulsive force is inversely proportional to not only the n th power of the distance but also the product of the density control function where two points locate. The order n is used as a parameter to reduce the influence of far points and adjust the range of repulsion. Distribution of points are so decided as to minimize the total potential energy of this repulsion system. However, this is a nonlinear system and the minimum is not easy to be obtained. Therefore, for practical use, iterative method is applied to get a locally minimum arrangement.

An example of the density control is shown in Fig.9. The area is surrounded by unit square and a circle of radius $r_0 = 0.1$ inside it. Fig.9(a) is the initial arrangement, Fig.9(b) is a converged result with constant density control function $d(r) = const.$ $r = \sqrt{x^2 + y^2}$ and Fig.9(c) is another result with density control function $d(r) = r_0/r$. The power n is set to 4 in these examples. Points are arranged near the vertex of the regular triangle each other. These arrangements look quite natural and suitable for BEM.

After the arrangement, we have to calculate an appropriate connectivity of the points to divide the area into triangle sub-areas. This procedure is called Delaunay triangulation. Delaunay triangulation is a very popular problem in the field of computational geometry and efficient algorithm has been investigated by Green and Sibson(1978), Bowyer (1981) and Watson (1981). Sugihara (1998) also studied this problem and published a good instruction book. Fig.9(d) shows triangle panels generated by Delaunay triangulation from the points in Fig.9(c). Takagi (1992) applied Delaunay triangulation to the adaptive mesh generator for FEM. Applications

of the Delaunay triangulation can be found in variety of areas from geography to computer graphics.

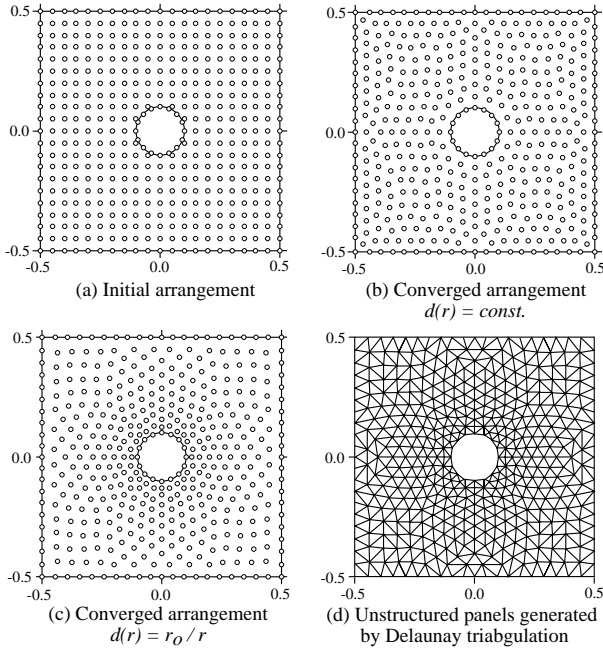


Fig.9 Example of density control of collocation points and Delaunay triangulation

3.4 REDUCTION OF CPU TIME AND MEMORY

For 3D NWTs, CPU speed and available memory on PC and EWS are still insufficient. Reduction of CPU time and required memory are urgent needs for practical 3D computation. Several ideas for the reduction were proposed.

3.4.1 Frozen coefficient method

Higher order time integration scheme is accurate, stable and faster because we can use large Δt . However, nonlinear simulation is still time consuming because influence matrices have to be updated every internal time steps. For example, RK method requires four internal steps to advance the simulation single time step Δt and so the influence matrices also updated four times per Δt . However, in the internal steps, change of boundary shape is usually very small and the change of influence matrix also assumed to be small. Ferrant (1998) used the same influence matrix through all the internal steps of RK and considerably accelerated the simulation of 3D nonlinear wave diffraction by a vertical cylinder without much loss of accuracy. Theoretically in RK method, we can simulate about four times faster with this method. This method is called "frozen coefficient method". Shirakura (2000) also used frozen coefficient for 3D floating body simulation.

3.4.2 Domain decomposition method

For nonlinear simulations of wave-train modulation, solitary wave propagation, focusing of wave packet, etc., long NWT based on domain decomposition method is

popularly used. Domain decomposition method is originally introduced to keep the accuracy of long NWT. In this method, long fluid domain is divided into adjacent sub-domains, then influence matrices are calculated for each sub-domain. At the interface of sub-domains, continuity of velocity potential and normal velocity of fluid are imposed as boundary conditions. In single domain method, influence matrices are full nonsymmetric and required memory size to store them is $\mathcal{O}(N^2)$, where N is total number of collocation points. Computational workload to solve the system is also $\mathcal{O}(N^2)$ or even larger. In domain decomposition method, total number of collocation points is increased but the matrix is block-diagonal instead of full nonsymmetric. Consequently, required memory size and CPU time to solve the system is reduced.

3.4.3 Multipole-accelerated BEM

For drastic acceleration of 3D NWT, multipole accelerated BEM is studied and general 3D codes to solve BIEs are under development now. Using multipole accelerated BEM, computational workload and memory requirement can be reduced to nearly $\mathcal{O}(N)$.

Korsmeyer et al.(1993,1996) developed FastLap code based on pre-conditioned, adaptive, multipole-accelerated algorithm. This code is a general solver for 3D Laplace problems on multiply-connected domains. FastLap supports only constant panel, now.

Multipole accelerated BEM is very promising technology. Development of general higher order 3D solver based on this technology will break new ground for practical 3D NWT.

4 WAVE GENERATION

Wave generation is one of the most basic function of NWT. This function is classified into two categories. One is physical wave generation which is imitative of wave maker in real wave tank. The other is artificial wave generation inapplicable in real wave tank.

4.1 PHYSICAL WAVE GENERATION

In physical wave generation methods, forced oscillated body surfaces are used as disturbance sources. Piston wave maker is the most well used wave generator for NWT. The merits of piston wave maker are as follows.

- (1) Piston wave maker is simple and easy to implement in NWT code.
- (2) The linear analytical solution of propagating wave by piston wave maker is known.

$$\phi(x, z, t) = \frac{4s \tanh kh \sinh kh}{\omega(2kh + \sinh 2kh)} \times \cosh k(z + h) \cos(kx - \omega t) \quad (95)$$

$$\eta(x, t) = \frac{4s \sinh^2 kh}{2kh + \sinh 2kh} \sin(kx - \omega t) \quad (96)$$

where s is the stroke of the piston, h is water depth, ω is frequency and k is wave number. This solution

can be useful to check the accuracy of wave generation function of NWT. The analytical solution is also useful for the reference value of damping zone, explained §5.3. (3) Piston wave maker can be used to generate not only deep water waves but also shallow water waves such as a solitary wave.

(4) Piston wave maker is suitable also for plunging wave generation. Fig.10 shows a plunging wave generated by a long stroke motion of piston wave maker.

Other than piston wave maker, various wave making surface can be used in NWT. Single flap, multi flaps, plunger type wave makers are popularly used. We can use any type of physical wave maker in NWT.

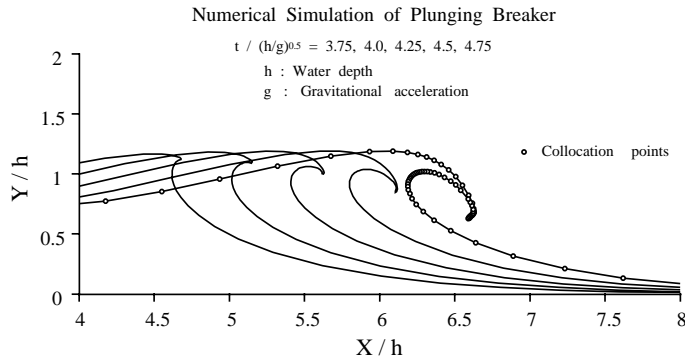


Fig.10 Simulation of plunging wave generated by a long stroke motion of piston wave maker

4.2 ARTIFICIAL WAVE GENERATION

In artificial wave making method, control surface is used as disturbance sources of wave generation. Usually, control surface is vertical and fixed in space. Analytical or numerical solution of propagating waves are used to specify the boundary value on it. Therefore the generated wave field is free from local waves. For small amplitude wave generation, we may use linear analytical solution. For large amplitude regular wave generation, we can use Stokes wave solution. For the generation of fully nonlinear regular wave, Ferrant (1998) used Rienecker and Fenton's solution (1981). In their solution, stream function of wave ψ is expanded into Fourier series

$$\psi(x, z) = B_0 z + \sum_{j=1}^N B_j \frac{\sinh jkz}{\cosh jkD} \cos jkx, \quad (97)$$

where coefficients are numerically determined so that ψ satisfies bottom and free surface boundary condition. Free surface shape is also determined numerically by iterative procedure. Mean current speed induced by nonlinear wave is vague in closed domain. Their method is adaptable to mean current speed and we can obtain the wave solution of zero mean current. This is another merit to apply their solution to NWT wave generation.

Allocation of pulsating singular point is another type of artificial wave making technique. Brorsen and Larsen (1987) used submerged pulsating source. Clément (1999a) used submerged spinning dipole which generates

an unsymmetrical one-sided wave field. Physical model of spinning dipole is spinning eccentric cylinder below free surface. Since spinning dipole is located inside of fluid domain, they used modified integral equation,

$$c(Q)\phi(Q) = \int_C \phi(P)u_n(P, Q) - u(P, Q)\phi_n(P)ds - m(t)\Re \left\{ \frac{\exp i\theta(t)}{z - z'} \right\}, \quad (98)$$

where $m(t)$ and $\theta(t)$ are intensity and direction of the dipole respectively.

Artificial wave generation is particularly useful for 3D NWT. The boundary condition on all control surfaces are given by single equation. Therefore, control of wave frequency, amplitude and direction is simple and easy.

5 WAVE ABSORPTION

To avoid wave reflection from the end of wave tank or side wall, every wave tank has wave absorbing devices. The simplest one is wave absorbing beach and elaborate one is active wave absorber. Similar to the real wave tank, NWTs have wave absorbing function. Wave absorbing method used in NWTs can be classified into three categories, (1) application of Sommerfeld radiation condition, (2) physical wave absorbing method used in real wave tank and (3) artificial wave absorbing method inapplicable in real wave tank.

5.1 SOMMERFELT-ORLANSKI RADIATION CONDITION

For the linear frequency domain computation, the wave radiation condition is indispensable to obtain unique solution. The radiation condition guarantees infinite extent of wave field from disturbance sources. Using the free surface Green function which satisfies the radiation condition, we can deal with infinite wave field. However in time domain nonlinear simulation, we can only deal with finite computational area. Sugihara and Isshiki (1980) studied applicability of Sommerfeld radiation condition to the linear frequency domain computation in closed computational area. They applied Sommerfeld radiation condition on a vertical control surface S_c at the finite distance from the disturbance and showed that the solution is unique and accurate compared with the exact solution of infinite area. We can expect that this is also true for time domain simulation in closed domain.

For time domain nonlinear simulation, application of Sommerfeld radiation condition is a little tricky. Here, a propagating wave to positive x direction is considered for simplicity. Then, Sommerfeld radiation condition can be written as

$$\phi_t + c\phi_x = 0, \quad (99)$$

where c is phase velocity of the wave. When this condition is applied to time domain numerical simulation,

this condition is usually called Sommerfeld-Orlanski radiation condition, Orlanski (1976). Jagannathan (1988) and Isaacson et al.(1991) used this method in their NWTs. In time domain simulation, we have to deal with transient phenomena. Therefore, value of c is not constant and have to be determined numerically so that eq.(99) is consistent with dynamic free surface boundary condition near S_c . Value of c is determined by substituting eq.(7) into eq.(99).

$$c = \left(\frac{1}{2} \nabla \phi \cdot \nabla \phi + \eta \right) / \phi_x, \quad (100)$$

where η is wave elevation at S_c . Suppose ϕ_x is known on S_c at a certain time step. Then, value of ϕ_t is obtained from eq.(99) and time integral of ϕ_t gives ϕ of next time step. Using ϕ as the boundary condition on S_c , BIE is solved and new ϕ_x is obtained. This is the basic sequence of Sommerfeld-Orlanski radiation condition applied to tank ends of NWTs.

5.2 PHYSICAL WAVE ABSORPTION

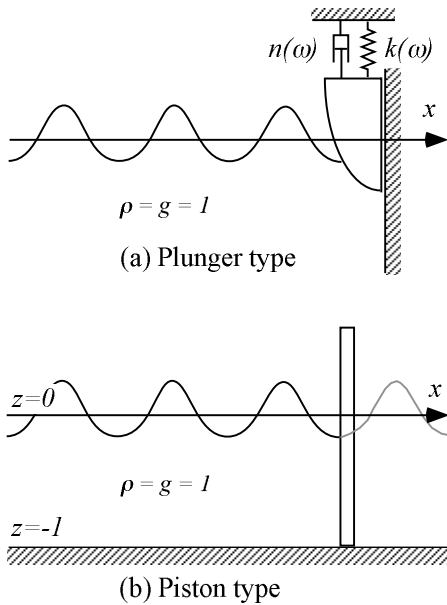


Fig.11 Plunger and piston wave absorber

Fig.11 is an illustration of physical wave absorbers. Type (a) is a plunger type wave absorber suspended by a linear damper $n(\omega)$ and a linear spring $k(\omega)$. Equation of the motion is

$$\begin{aligned} \{M + m(\omega)\} \ddot{z}(t) + N(\omega) \dot{z}(t) + Cz(t) \\ = F_w(t) - \{n(\omega) \dot{z}(t) + k(\omega) z(t)\}, \end{aligned} \quad (101)$$

where M is mass of absorber, $m(\omega)$ is added mass, $N(\omega)$ is wave damping coefficient, C is heave restoring coefficient and F_w is wave exciting force. Bessho (1973) studied the optimal wave absorbing condition under the linear assumption and derived

$$n(\omega) = N(\omega), \quad (102)$$

$$k(\omega) = \{M + m(\omega)\} \omega^2 - C. \quad (103)$$

When $n(\omega)$ and $k(\omega)$ satisfy the above condition, the plunger works as a perfect absorber for linear regular

waves. Naito et al.(1984,1987a,1987b) studied absorption of regular and irregular waves by plunger type absorber and developed a efficient feed forward control system. Theoretically, we can use the same idea to develop plunger type wave absorber in NWTs. In the real world, friction of mechanical part and noise in electric part are always obstacles to improve efficiency of absorber. However in NWT, we can build ideal absorber free from these obstacles.

Fig.11 (b) is a piston type wave absorber. The motion of piston is controlled in a manner so as to be invisible to the waves. In other word, piston is controlled to generate imaginary waves on the back side just as if the waves pass through. The fundamental difference between Sommerfeld-Orlanski radiation condition (99) and piston wave absorber is flexibility of flux on the wave absorbing boundary. Since ϕ_x is constant on the piston surface, we can expect that piston wave absorber is suitable for long wave absorption. For long wave absorption, we can control velocity of the piston by the same sequence of Sommerfeld-Orlanski radiation condition explained in §5.1.

Assuming the infinite long wave, Clément (1996a) derived another absorbing condition on the piston,

$$\frac{\partial \phi}{\partial x} = F_D = \int_{-h}^{\eta} -\phi_t ds, \quad (104)$$

where F_D is hydrodynamic force, η is wave elevation at the piston and $h = 1$ is water depth (used as principle length in the condition). In this condition, hydrodynamic force is used as input signal. The wave absorption coefficients by this method are approximately 97% for $\lambda/h = 12$, 60% for $\lambda/h = 3$ and 20% for $\lambda/h = 1$, where λ is wave length. Clément showed the combination use of this piston wave absorber and damping zone explained in §5.3 covers both long and short wave ranges. The numerical implementation of this absorbing condition was reported by Grilli and Horillo (1997). Denoting the position, velocity and acceleration of the piston as x_p , \dot{x}_p and \ddot{x}_p respectively, piston absorber is controlled by following sequence.

$$\left. \begin{aligned} \dot{x}_p(t + \Delta t) &= \{F_D(t) + \dot{x}_p(t)\} / 2 \\ x_p(t + \Delta t) &= x_p(t) + \dot{x}_p(t) \Delta t \\ &\quad + \ddot{x}_p(t) \Delta t^2 / 2 \\ \phi_x(t + \Delta t) &= \dot{x}_p(t + \Delta t) \\ \phi_{tx}(t + \Delta t) &= \ddot{x}_p(t + \Delta t) \\ &\quad - \dot{x}_p(t + \Delta t) \phi_{zz}(t + \Delta t) \end{aligned} \right\}, \quad (105)$$

where the moving average in the first equation is introduced to avoid numerical oscillation, and \ddot{x} is calculated as second-order finite difference approximation.

More sophisticated control methods were studied and are still in development. Skourup and Schaffer (1998) studied active absorption of multidirectional waves by piston type wave absorber and developed 3D active wave absorption control system, 3D-AWACS. Chatry et al.(1999) applied Kalman filter to self-adaptive control of piston wave absorber.

5.3 ARTIFICIAL WAVE ABSORPTION

Artificial wave absorbing methods are called as sponge layer, artificial beach or damping zone. In this paper, these methods are generally referred as damping zone. In damping zone, artificial damping terms are added to free surface boundary conditions.

In the linear problem, Nakos et.al. (1993) reported excellent performance of their proposed damping zone. They added a damping term called Newtonian cooling term only in the kinematic boundary condition. Kashiwagi (1996) extended their idea to fully nonlinear problem and gave following kinematic boundary condition,

$$\frac{Dx}{Dt} = \phi_x, \quad \frac{Dz}{Dt} = \phi_z - 2\nu z - \nu^2 \phi, \quad (106)$$

where ν is nonzero inside the damping zone $[x_0, x_1]$ and given by

$$\nu(x) = \begin{cases} 3C_s(x - x_0)^2/|x_1 - x_0|^3, & x \in [x_0, x_1] \\ 0, & \text{otherwise} \end{cases} \quad (107)$$

Kashiwagi set coefficient C_s to 1.2 for his simulation.

Cointe et al. (1990) developed a powerful damping zone technique for their 2D NWT. In the damping zone, following absorbing free surface boundary condition is applied.

$$\frac{D\phi}{Dt} = -z + \frac{1}{2}\nabla\phi \cdot \nabla\phi - \nu(x_e)(\phi - \phi_e) \quad (108)$$

$$\frac{D\mathbf{x}}{Dt} = \nabla\phi - \nu(x_e)(\mathbf{x} - \mathbf{x}_e), \quad (109)$$

where \mathbf{x} is coordinate of a collocation point on free surface. Damping coefficient $\nu(x)$ is given by

$$\nu(x) = \begin{cases} \alpha\omega[(x - x_0)/\lambda]^2, & x \in [x_0, x_0 + \beta\lambda] \\ 0, & \text{otherwise} \end{cases} \quad (110)$$

where ω and λ are frequency and length of wave respectively. Strength and length of the damping zone are controlled by dimensionless parameters α and β , respectively. Appropriate value of these parameters are found to be $\alpha \approx 1$, $\beta \geq 1$. The terms ϕ_e and $\mathbf{x}_e = (x_e, z_e)$ in eq.(108) and (109) are reference values. This damping terms absorb differences between reference values and simulated values. When the damping zone is used as a simple absorber, reference values of calm condition (i.e. $\phi_e = 0$, $z_e = 0$) are used. If reference values of a propagating wave are given, this damping zone let only this wave pass through. Using this characteristic, we can compose an absorbing wave maker with any wave generator explained §4. Reference values are obtained from a numerical simulation of wave generation. For practical use, analytical solution such as eq.(95), (96) can be a substitute. Rienecker and Fenton's solution (1981) is also a good substitute for reference values.

Fig.12 shows the effect of the wave damping zone. Wave absorbing performance of this damping zone is excellent and reflection coefficient from the damping zone

is less than 2 % for deep water waves. This value is much better than wave absorbing beaches used in the real wave tanks.

For another wave absorbing methods, Romate's (1992) review paper of absorbing boundary conditions is a good reference.

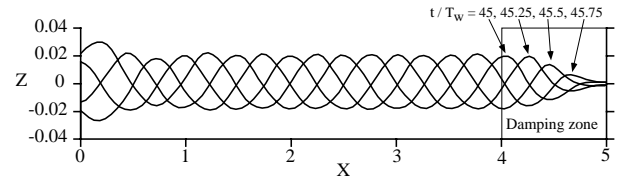


Fig.12 Wave absorption by wave damping zone

6 HYDRODYNAMIC FORCES

Computation of nonlinear hydrodynamic forces is one of the most important function of NWT. Hydrodynamic forces are obtained from pressure integral on wet body surface. Here, let us refer Bernoulli's pressure equation (34), again. The first term ϕ_t is the first order quantity and essentially important. The second term $\frac{1}{2}\nabla\phi \cdot \nabla\phi$ is the second order quantity and very small usually. The third term z is the first order quantity and as important as the first term. But, this term is so easy to evaluate that there is no doubt in accuracy. Thus, accuracy of ϕ_t directly affects to the accuracy of hydrodynamic forces.

As explained in §2.5, we can solve the implicit BIE of ϕ_t to calculate instantaneous floating body motions. In the similar way, ϕ_t on fixed body or forced oscillated body can be also give as the solution of BIE. On such a motion prescribed body surface, since body acceleration α is known, body surface boundary condition is explicitly given by eq.(15). Then BIE of ϕ_t is solved explicitly. Of course, the influence matrices for ϕ_t are the same as those for ϕ , and so the inverse matrices have been obtained when the BIE of ϕ is solved. Therefore, computational workload to calculate ϕ_t is very small.

Kashiwagi (1996) computed hydrodynamic forces on vertically oscillated 2D elliptic and wedge. BIE of ϕ_t was solved. The computed time history of hydrodynamic forces were compared with linear theoretical value by time domain Green function method and measurements. Fourier analysis was applied to these time histories and results were compared up to third order. All of these results were in excellent agreement and the validity of the calculation method was confirmed. Tanizawa and Clément (2000) conducted benchmark test of fully nonlinear radiation problem by sinusoidal heaving motion of a 2D wedge. Among seven contributors, four contributors used fully nonlinear NWT based on BEM. Although these four NWTs were developed independently, the simulated hydrodynamic forces showed very good agreement each other. BIE of ϕ_t was solved in all NWTs. Results of Fourier analysis were also compared and the mutual agreement was confirmed up to third order. Following the radiation problem, Tanizawa (2001) conducted benchmark test of diffraction problem by 2D

Lewis form body. Two contributors used BEM and BIE of ϕ_t was solved to compute pressure. Simulated hydrodynamic forces were compared with measurements and agreement among them was confirmed also up to third order by Fourier analysis. Celebi et al.(1998) also solved BIE of ϕ_t to compute wave diffraction forces on a truncated vertical cylinder in their 3D NWT.

If problems are restricted to hydrodynamic forces on motion prescribed body surface, backward finite difference of ϕ can be used to calculate ϕ_t . In fully nonlinear simulation, collocation points on body surface are moving in time and backward finite difference is applied to approximate semi-Lagrangian derivative $d\phi/dt$ in eq.(25). Therefore, accurate value of $v(P)$ and $\nabla\phi$ on the body surface are necessary to calculate ϕ_t . In the past many NWTs, this finite difference approximation method was popularly used. However, this method is considered to be outdated and will be replaced by BIE solution of ϕ_t .

7 FLOATING BODY MOTIONS

Simulation of nonlinear floating body dynamics is the most interesting application of NWTs. As explained in §2.5, the bases of floating body simulation were established and their potentialities were demonstrated by simulations of various nonlinear floating body motions in 2D NWT. For example, Tanizawa (1998) applied 2D NWT to the study on chaotic roll motions of a unstable round rectangular body with small negative GM. Fig.13 shows an example of simulated roll motions in a long regular wave, $\lambda/B \sim 13.5$. Stable heel angle of this body is $\pm 4degree$. As the ratio between wave height and the draft H_w/d becomes larger, the simulated roll response changes completely. Chaotic responses are essential in this example. Simulation of such a nonlinear motions well demonstrate the capability of NWT.

The next step is development of 3D NWT for the simulation of floating body motions. Berkvens (1998) developed a cylindrical 3D NWT based on implicit boundary condition method and simulated free heaving motion of homogeneous sphere which was released in a position slightly above its equilibrium. Damping zone was applied along the circumference of NWT. Shirakura et al. (2000) also developed similar cylindrical 3D NWT based on implicit boundary condition method and simulated free heaving motion of a sphere. Conservation law of fluid volume, energy and momentum were checked by eq.(62) ~ (68) and the error was confirmed to be very small. Ikeno (2000) developed a rectangular 3D NWT and simulated transient motion of moored barge in a regular wave. The results were compared with experimental data and the close agreement was reported.

8 CONCLUSION

In the field of naval architecture and ocean engineering, we have to solve variety of problems concerning on free surface waves, hydrodynamic forces act on ships and ocean platforms, seakeeping performance of running

ship, long period motions of moored ocean platforms and etc. For design of ships and ocean platforms, linear theories are the most powerful tool now and may be also in future. This is a quite reasonable guess because responses of floating bodies to waves are mostly linear and weak nonlinear components merely superposed on them. However, recent social and environmental changes claim us further safety and economy. Seakeeping performance and safety assessment of ships and ocean structures in heavy storms are particularly important social and environmental issue and further accurate estimation methods are demanded. To meet such a requirement, we have to adopt advanced technologies and develop more rational tools universally applicable to not only linear but also fully nonlinear waves and floating body dynamics.

NWT is one of the promising tools and expected to substitute real wave tanks. We can apply NWT to variety of simulations such as fully nonlinear free surface waves, wave radiation by oscillated body, wave and fixed body interaction and floating body dynamics. In near future, we will be able to simulate wave tank experiment on desktop computer and mainly use NWT not only for research but also for design. At that time, real wave tank will be used to complement or check the numerical results by NWT. NWT will be applied to design ship hull form below and above water, mooring system of ships and ocean platforms, wave energy power plant, wave maker and absorber of real wave tank and etc. However, present state of NWT is still complement of real wave tank. Continuous effort should be made to develop practical 3D NWTs.

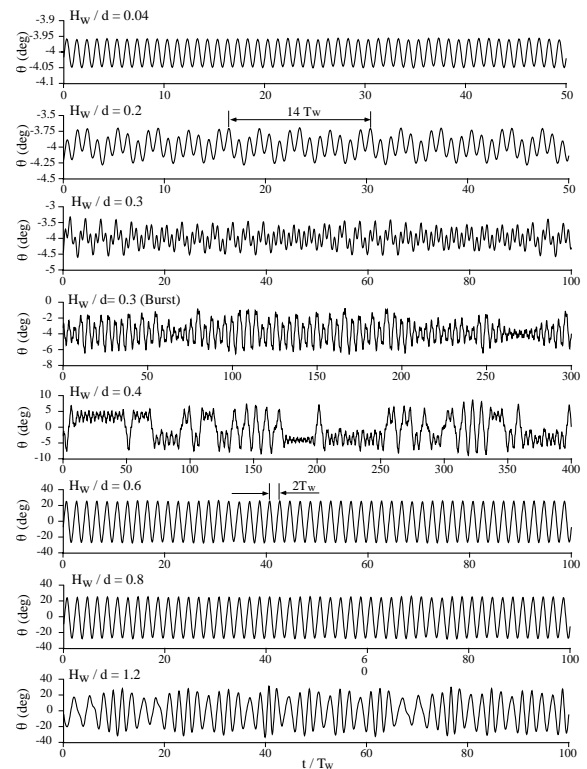


Fig.13 Simulated chaotic roll motions of a weakly unstable 2D floating body in a regular wave

REFERENCES

- Abramowitz, M. and Stegun, I.A., (1964), "Handbook of mathematical functions", *Dover Publications*, pp.887
- Barrett, R., Berry, M., Chan, T.F., Dammel, J., Donato, J.M., Dongarra, J., Eijkhout, V., Pozp, R., Romine, C., Van der Vorst, H., (1994), "Templates for the solution of linear systems : Building blocks for iterative methods", *Published by SIAM*, Philadelphia, PA, pp.19-21
- Beck, R.F., Cao, Y. and Lee, T.H., (1993), "Fully nonlinear water wave computations using the desingularized method", *Proc. of 6th Int. Conf. on Ship Hydro.*, pp.3-20
- Berkvens, P.J.F. (1998), "Floating bodies interacting with water waves", *Ph.D. thesis*, University of Twente, The Netherlands, pp.1-161
- Bessho, M. (1973) "Feasibility study of floating wave absorber", *Proc. 34th JTTC*
- Boo, S.Y. and Kim, C.H., (1996), "Fully nonlinear diffraction due to a vertical circular cylinder in a 3-D HOBEM Numerical Wave Tank", *Proc. 6th ISOPE Conf.*, Los Angeles, USA, Vol.3, pp.76-84
- Boo, S.Y. and Kim, C.H., (1997), "Nonlinear irregular waves and forces on truncated vertical cylinder in a numerical wave tank", *Proc. 7th ISOPE Conf.*, Honolulu, Hawaii, Vol.3, pp.23-30
- Bowyer, A., (1981), "Computing Dirichlet tessellation", *The Computer Journal*, vol.24, No.2, pp.162-166
- Brorsen, M. and Larsen, J. (1987), "Source generation of nonlinear gravity waves with the boundary integral equation method", *Coastal Eng.*, Vol.11, pp.93-113
- Cao, Y., Beck, R. and Schultz, W.W. (1994), "Nonlinear motions of floating bodies in incident waves", *9th Workshop on Water Waves and Floating Bodies*, Kuju, Oita, pp.33-37
- Celebi, M.S., Kim, M.H. and Beck, R.F. (1998), "Full nonlinear 3-D numerical wave tank simulation", *J. Ship Research*, Vol.42, No.1, pp.33-45
- Chatry, G., Clément, A.H. and Gouraud, T. (1998), "Self-adaptively control of a piston wave-absorber", *Proc. 8th ISOPE Conf.*, Montréal, Vol.1, pp.127-133
- Chatry, G., Clément, A.H. and Sarmiento, A.J.N.A. (1999), "Simulation of self-adaptively controlled OWC in a nonlinear numerical wave tank", *Proc. 9th ISOPE Conf.*, Brest, Vol.3, pp.290-296
- Clément, A.H., (1996a), "Coupling of two absorbing boundary conditions for 2D time-domain simulations of free surface gravity waves", *J. Comp. Physics*, Vol.126, pp.139-151
- Clément, A.H., (1996b), "Dynamic nonlinear response of OWC wave energy devices", *Proc. 6th ISOPE Conf.*, Los Angeles, Vol.1, pp.91-96
- Clément, A.H., (1999a), "The spinning dipole : an efficient unsymmetrical numerical wavemaker", *Proc. 14th Int. Workshop on Water Waves and Floating Bodies*, Port Huron, Michigan
- Clément, A.H., (1999b), "Benchmark test cases for numerical wave absorption", *Proc. 9th ISOPE Conf.*, Vol.3, pp.266-289
- Cointe, R., Geyer, P., King, B., Molin, B. and Tramoni, M. (1990), "Nonlinear and linear motions of a rectangular barge in perfect fluid", *Proc. of the 18th Symp. on Naval Hydro.*, Ann Arbor, Michigan, pp.85-98
- Craven, P. and Wahba, G. (1977), "Smoothing noisy data with spline functions, Estimating the correct degree of smoothing by the method of generalized cross-validation", *Technical Report*, Department of statistics, University of Wisconsin, No.445, pp.1-46
- Dommermuth, D.G. and Yue, D.K.P., (1987), "Numerical simulations of nonlinear axisymmetric flows with a free surface", *J. Fluid Mech.*, Vol.178, pp.195-219
- Dommermuth, D.G., Yue, D.K.P., Lin, W.M., Rapp, R.J., Chan, E.S. and Melville, W.K., (1988), "Deep-water plunging breakers: a comparison between potential theory and experiments", *J. Fluid Mech.*, Vol.189, pp.423-442
- Ferrant, P., (1998), "Runup on a cylinder due to waves and current: Potential flow solution with fully nonlinear boundary conditions", *Proc. 8th ISOPE Conf.*, Vol.3, pp.332-339
- Ferrant, P., (1999), "Fully nonlinear diffraction of regular waves by a multi-column structure", *Proc. 9th ISOPE Conf.*, Vol.3, pp.337-344
- Green, P.J. and Sibson, R., (1978), "Computing Dirichlet tessellation in the plane", *The Computer Journal*, vol.21, No.2, pp.168-173
- Grilli, S. and Horrillo, J., (1997), "Numerical generation and absorption of fully nonlinear periodic waves", *J. Eng. Mech.*, ASCE, Vol.123, pp.1060-1069
- Grilli, S., Guyenne, P. and Dias, F. (2000), "Modeling of overturning waves over arbitrary bottom in 3D numerical wave tank", *Proc. 10th ISOPE Conf.*, Vol.3, pp.221-228
- Hyman, J.M. and Naughton, M.J., (1985), "Static zone methods for tensor-product grids", *Lectures in Applied Mathematics*, AMS, Providence, Vol.22, pp.321-343
- Ikeno, M. and Matsuyama, M., (1996), "Two dimensional numerical model for fully nonlinear interaction between moored floating structure and tsunami", *Rep.*

- Abiko Research Lab.*, Central Res. Inst. Electric Power Industry, U95043, pp.1-43
- Ikeno, M., (2000), "A numerical model for 3-D floating body motion in nonlinear waves using the BEM", *Proc. 10th ISOPE Conf.*, Vol.3, pp.201-213
- Isaacson, M. and Cheung, K. F. (1991), "Second order wave diffraction around two-dimensional bodies by time-domain method", *Appl. Ocean Res.*, Vol.13, No.4, pp.175-186
- Jagannathan, S. (1988), "Nonlinear free surface flows and an application of the Orlandi boundary condition", *Int. J. for Numer. Methods in Fluids*, Vol. 8, pp.1051-1070
- Kang, C.G., and Gong, I.Y., (1990), "A numerical solution method for three-dimensional nonlinear free surface problems", *Proc. of the 18th Symp. on Naval Hydro.*, Ann Arbor, Michigan., pp.427-438
- Kashiwagi, M. (1996), "Full-nonlinear simulations of hydrodynamic forces on a heaving two-dimensional body", *J. Soc. Nav. Arch. Japan*, Vol.180, pp.373-381
- Kashiwagi, M. (1998), "Nonlinear simulations of wave-induced motions of a floating body by means of MEL method", *Proc. of 3rd Int. Conf. on Hydrodynamics*, Seoul.
- Kihara, H., (1998), "Research of nonlinear fluid force acts on slender ship with large amplitude motions (in Japanese)", *Ph.D thesis, Osaka Univ.*, pp.1-142
- Kim, C.H., Clément, A.H. and Tanizawa, K., (1999), "Recent research and development of numerical wave tanks - A review", *Int. J. Offshore and Polar Eng.*, Vol.9, No.4, pp.241-256
- Korsmeyer, F.T., Yue, D.K.P., Nabors, K. and White, J. (1993), "Multipole accelerated preconditioned iterative methods for three-dimensional potential problems", *Proc. of BEM 15*, pp.517-527
- Korsmeyer, F.T., Nabors, K. and White, J. (1996), "FastLap Version:2", *Users guide of FastLap*, MIT Research Lab. of Electronics, pp.1-26
- Lancaster, P. and Salkauskas, K., (1986), "Curve and surface fitting", *Academic Press*, pp.87-111
- Lin, W.M. and Yue, D., (1991), "Numerical solutions for large-amplitude ship motions in the time domain", *Proc. 18th Symp. on Naval Hydro.*, pp.41-66
- Longuet-Higgins, M.S. and Cokelet, E., (1976), "The deformation of steep surface waves on water I. A numerical method of computation", *Proc. Roy. Soc. ser.A350*, pp.1-26
- Nabors, K., Phillips, J., Korsmeyer, F.T. and White, J.: "Domain-Based Parallelism and Problem Decomposition Methods in Science and Engineering", *SIAM*, edited by Keyes, D.E., Saad, Y. and Truhlar, D.G.
- Naito, S., Nakamura, S. and Furukawa, H. (1984), "Wave energy absorption of irregular waves", *J. Kansai Soc. Nav. Arch. Japan*, vol.194, pp.25-31
- Naito, S., Huang, J., Nagata, M. and Nakamura, S. (1987a), "Research on perfect absorption of regular wave with the terminal device", *J. Kansai Soc. Nav. Arch. Japan*, vol.205, pp.29-36
- Naito, S., Huang, J., and Nakamura, S. (1987b), "Research on the absorb-making of irregular waves with the terminal device", *J. Kansai Soc. Nav. Arch. Japan*, vol.207, pp.25-32
- Nakos, D.E., Kring, D., and Scavounos, P.D., (1993), "Rankine panel methods for transient free surface flows", *Proc. 6th Int. Conf. on Num. Ship Hydro*, Iowa, pp.29-48
- Orlandi, I. (1976), "A simple boundary condition for unbounded hyperbolic flows", *J. of Comput. Phys.*, Vol. 21, pp.251-269
- Rienecker, M.M. and Fenton, J.D. (1981), "A Fourier approximation method for steady water waves", *Journal of Fluid Mechanics*, Vol.104, pp.119-137
- Romate, J.E., (1992), "Absorbing boundary conditions for free surface waves", *J. of Comp. Physics*, Vol.99, pp.135-145
- Saad, Y. and Schultz, M.H., (1985), "A generalized minimal residual algorithm for solving nonsymmetric linear systems", *SIAM J. Sci. and Stat. Comp.*, Vol.7, pp.417-424
- Sen, D., (1993), "Numerical simulation of motions of two-dimensional floating bodies", *Journal of Ship Research*, Vol.37, pp.307-330
- Shirakura, Tanizawa, Naito (2000), "Development of 3-D fully nonlinear numerical wave tank to simulate floating bodies interacting with water waves", *Proc. 10th ISOPE Conf.*, Seattle, Vol.3, pp.253-262
- Skourup, J. and Schäffer, H.A. (1998), "Simulation with 3-D active absorption method in numerical wave tank", *Proc. 8th ISOPE Conf.*, Montréal, Vol.3, pp.248-255
- Sugihara, K., (1998), "Computational geometry and programming", *The iwanami computer science series*, pp.1-402
- Sugiura, M. and Isshiki, H., (1980), "Sommerfeld's radiation condition associated with water waves and its application for numerical calculation", *J. Kansai Soc. Nav. Arch. Japan*, vol.156, pp.67-74
- Takagi, K., Naito, S. and Nakamura, S. (1985), "Computation of nonlinear hydrodynamic forces on two-dimensional body by boundary element method", *J. Kansai Soc. Nav. Arch. Japan*, Vol.197, pp.31-38

- Takagi,K.,(1992), "A Finite element method with an adaptive mesh refinement procedure for numerical calculation of three dimensional unsteady free surface flows", *J. Kansai Soc. N. A. Japan*, No.217, pp.77-83
- Tanizawa,K. and Sawada,H., (1990), "A numerical method for nonlinear simulation of 2-D body motions in waves by means of BEM", *J. Soc. Nav. Arch. Japan*, Vol.168, pp.223-228
- Tanizawa,K., (1995a), "A Nonlinear Simulation Method of 3-D body Motions in Waves (1st Report)", *J. Soc. Nav. Arch. Japan*, vol.178, pp.179-191
- Tanizawa,K., (1995b), "On the paneling technique for the nonlinear simulation of free surface waves", *Proc. of Symp. on Nonlinear and Free Surface Flow*, Vol.4, pp.37-40
- Tanizawa,K., (1996a), "Nonlinear simulation of floating body motions in waves", *Proc. of 6th ISOPE conference*, Los Angeles, California, Vol.3, pp.414-420
- Tanizawa,K. (1996b), "Long time fully nonlinear simulation of floating body motions with artificial damping zone", *J. Soc. Nav. Arch. Japan*, vol.180, pp.311-319
- Tanizawa, K. and Naito, S. (1997a), "A study on parametric roll motions by fully nonlinear numerical wave tank", *Proc. of 7th ISOPE Conf.*, Honolulu, Hawaii, vol.3, pp.69-75
- Tanizawa,K., (1997b), "Nonlinear theory of wave-body interaction based on acceleration potential and its application to numerical simulation (in Japanese)", *Ph.D thesis, Osaka Univ.*, pp.1-127
- Tanizawa, K. and Naito, S. (1998), "An application of fully nonlinear numerical wave tank to the study on chaotic roll motions", *Proc. of 8th ISOPE Conf.*, Montréal, Vol.3, pp.280-287
- Tanizawa, K. and Clément, A.H. (2000), "Report of the 2nd workshop of ISOPE NWT group, Benchmark test cases of radiation problem", *Proc. of 10th ISOPE Conf.*, Seattle, Vol.3, pp.175-184
- Van Daalen, E.F.G. (1993), "Numerical and Theoretical Studies of Water Waves and Floating Bodies", *Ph.D. thesis*, University of Twente, The Netherlands, pp.1-285
- Vinje, T. and Brevig, P. (1981a), "Nonlinear Ship Motions", *Proc. of the 3rd. Int. Conf. on Num. Ship Hydro.*, pp.IV3-1-IV3-10
- Vinje,T., and Brevig,P., (1981b), "Nonlinear, two-dimensional ship motions", *Norwegian Hydrodynamic Laboratories, Report R- 112.81,Trondheim, Norway.*, pp.1-97
- Wahba,G., (1981), "Bayesian confidence intervals for cross validated smoothing spline", *Technical Report*, Department of statistics, University of Wisconsin, No.645 pp.1-60
- Watson,D.F.,(1981), "Computing the n -dimensional Delaunay tessellation with application to Voronoi polytopes", *The Computer Journal*, vol.24, No.2, pp.167-172
- Wu, G.X. and Eatock Taylor, R. (1996), "Transient motion of a floating body in steep water waves", *Proc. of 11th Int. Workshop on Water Waves and Floating Bodies*, Hamburg
- Xi,H. and Yue.,D.K.P., (1992), "Numerical study of three dimensional overturning waves", *Proc. 7th Workshop on Water Waves and Floating Bodies*, pp.303-307
- Zhang,S., Yue,D.K.P. and Tanizawa,K., (1996), "Simulation of plunging wave impact on a vertical wall", *J. Fluid Mech.*, Vol.327, pp.221-254
- Zou,J. and Kim,C.H., (1996), "A note on preconditioned GMRES solver", *Proc. 6th ISOPE Conf.*, Los Angeles, USA, vol.3, pp.44-49